A Heat Transfer Study of Using Geothermal Energy to Stimulate Oil Wells in the Tuscaloosa Marine Shale Reservoir

He Zhang

A Dissertation Presented to the Graduate Faculty
in Partial Fulfillment of the Requirements for the Degree
Doctor of Philosophy

University of Louisiana at Lafayette
Fall 2022

APPROVED:

Boyun Guo, Chair
Department of Petroleum Engineering

Ning Liu
Department of Petroleum Engineering

Yin Feng
Department of Petroleum Engineering

Nelson Chavez
Department of Petroleum Engineering

Tanvir Rahman Faisal
Department of Mechanical Engineering

Mary Farmer-Kaiser
Dean of the Graduate School

Abstract

This paper presents a review of oil production performance of Tuscaloosa Marine Shale (TMS) wells and proposes a new method to improve TMS well productivity using geothermal energy stimulation. The average oil production rate of TMS wells was found to decline from a few hundred barrels per day to about 20 stb/day in the first 5 years of production. This annual decline rate is approximately 23%, which is same as the decline rate in the Eagle Ford Shale (EFS) but higher than that in the Williston and Permian shales. Result of mathematical modeling showed that use of y-shaped well couples to transfer the geothermal energy in a deeper depth to the TMS pay zone can reduce oil viscosity from 0.5 cp to 0.22 cp. This reduction in oil viscosity is translated to an increase of well initial oil production rate from 140 stb/day to 320 stb/day. The flow rate of work fluid is a key factor affecting the heat transfer from geothermal zones to heat dissipator wellbores. While high flow rate brings more heat from the geothermal zone to the dissipator wellbore, the temperature drop along the wellbore decreases slightly, reducing the time of heat transfer. Long oil production wellbores should be drilled to ensure adequate time for heat transfer. The heat transfer from the heat dissipator wellbore to the oil reservoir is a slow process due to the low-thermal conductivity of reservoir rock and fluids. It should take about 2 years for the reservoir temperature to increase from 99.3^{o}C to 110^{o}C everywhere within a radial distance of 10 m. However, the temperature in the vicinity of the heat dissipator wellbore should increases quickly and stabilize at high level, suggesting no need to wait for heat transfer prior to oil production from the production wellbore if the production wellbore is placed in a few meters to the heat dissipator wellbore.

To my parents, Laicheng Zhang & Chunling Yan
To my wife, Changlu Liang, and
To my kids, Enwei Zhang & Edmond L. Zhang.

Acknowledgments

I would like to acknowledge and give my warmest thanks to my advisor Dr. Boyun Guo, Director of the Centre for Optimization of Petroleum Systems, for giving me the opportunity to complete the Ph.D. program at the University of Louisiana at Lafayette. His guidance and advice carried me through all the stages of writing my project. His support and help made me, step by step, like to do research, and then gradually be on the right path from a research newbie to a real academic researcher. Also, I would like to thank all the members of my Ph.D. advisory committee, Dr. Yin Feng, Dr. Ning Liu, Dr. Nelson Chavez, Dr. Tanvir Faisal, and Dr. Yilin Mao for letting my defense be an enjoyable moment, and for the brilliant comments and suggestions in revising and optimizing my dissertation.

This dissertation is supported by the Tuscaloosa Marine Shale Lab (project number DE-FE0031575) from the Department of Energy National. I would like to thank the PI, Dr. Mehdi Mokhtari, and Dr. Ning Liu for inviting me to join the research team and supporting me.

I would also thank Dr. Douglas Winslow Cooper and my child Enwei Zhang for their careful proofreading, as well as Dr. Cooper's smart suggestions for this work. He and many others have helped and encouraged me to complete this dissertation and rekindle my academic interests.

Finally, I would like to thank my parents and my wife for their continuous support and understanding when undertaking my research and writing project. Without their support, I cannot seek and realize my research dream. During my Ph.D. program, my wife came to Lafayette with me and encouraged me to go through all the difficult days. I would also like to thank all my friends in Lafayette for helping me.

Table of Contents

List of Tables

List of Figures

List of Abbreviations

A_{csg}	Inner cross-sectional area of casing pipe in m^2
A_p	Inner cross-sectional area of pipe open for fluid flow in m^2
B_o	Oil formation volume factor
C	Heat capacity of the rock in J/kg-^oC
C_p	Heat capacity of the work fluid in J/kg-^oC
C_{pl}	Heat capacity of the fluid inside the wellbore in J/kg-^oC
C_{ps}	Rock heat capacity in J/kg-^oC
D_{csg}	Outer diameter of the casing (inner diameter of cement sheath) in m
DMAIC	Define, Measure, Analyze, Improve, and Control
D_p	Outer diameter of work pipe in m
d_p	Inner diameter of work pipe in m
e	Exponential function
EIA	Energy Information Administration
Ei(s)	Exponential integral
h	Pay zone thickness in ft
K	Rock thermal conductivity in W/m-^oC
K_a	Thermal conductivity of annulus fluid in W/m-^oC
K_c	Thermal conductivity of cement sheath in W/m-^oC
k_f	Fracture permeability in md
k_m	Matrix permeability in md
K_p	Thermal conductivity of pipe in W/m-^oC

L	Length of the wellbore section in meter
$L4$	Distance from the fluid entry point (length of Section IV) in m
$\dot{m}_p$	Mass flow rate of work fluid in kg/s
n_f	Number of fractures
$\bar{p}$	Average formation pressure in psia
p_w	Wellbore pressure in psia
Q	Heat source in W/ m^3
q_a	Lateral heat exchange through the casing pipe due to conduction in J
Q_o	Oil production rate in stb/d
Q_p	Flow rate in m^3/s
q_p	Lateral heat exchange through the work pipe due to conduction in J
$Q_{p,chng}$	External heat exchange through work pipe in J
$Q_{p,in}$	Heat source due to convection in J
$Q_{p,out}$	Flow out heat energy due to convection in J
$Q_{p,chng}$	External heat exchange through work pipe in J
q_{rw}	Rate of flow of heat per unit time per unit area of wellbore in J/s-m^2
r	Distance from the wellbore center line in m
r_s	Rock density in kg/m^3
r_w	Radius of the wellbore in meter
S_f	Fracture spacing in ft
t_c	Thickness of cement sheath in m
t	Time in second

T	Temperature in ^oC
T_a	Temperature in the annulus in ^oC
t_a	Thickness of annulus in m
T_{a1}	Fluid temperature in the annulus of Section I in ^oC
T_c	Thickness of cement sheath in m
T_g	Geothermal temperature at target depth in ◦C
T_{g3}	Average geo-temperature in the Section III in ^oC
T_{g4}	Average geothermal temperature at the depth of section IV in ^oC
T_i	Initial reservoir temperature in ^oC
T_{in}	Fluid temperatures in ℃ at the inlet of the wellbore
TMS	Tuscaloosa Marine Shale
TOC	Total organic content
T_{out}	Fluid temperatures in ℃ at the outlet of the wellbore
T_p	Temperature in the pipe in ^oC
u	Velocity field in m/s
U.S.	United States
w	Average fracture width in inch
x_f	Fracture half-length in ft
ρ_L	Liquid density in kg/m^3
β	Thermal diffusivity constant
ρ/ρ_s/Rho	Solid density in kg/m^3
μ	Fluid viscosity in cp

ΔL	Infinitesimal length in m
Δt	Infinitesimal time period in second

Chapter 1: Introduction

The recovery of the oil in oil shale deposits is important to the economy of our nation's energy supplies. This recovery can be increased if the oil can be heated to make oil flow easily. This thesis addresses the use of y-shaped well couples and geothermal heating to accelerate the recovery of oil from the Tuscaloosa Marine Shale (TMS) Trend. Various engineering parameters are investigated for system optimization to maximize oil production and recovery.

1.1 Literature Review

1.1.1 Overview of Tuscaloosa Marine Shale

The Tuscaloosa Marine Shale, located in central Louisiana and western Mississippi along the Gulf Coast, is the hydrocarbon source rock in the Tuscaloosa Group. The Tuscaloosa Group is the fifth transgressive-regressive cycle of the Late Cretaceous section. The TMS belongs to the maximum-transgressive deposits (Mancini and Puckett, 2002).

The Tuscaloosa Group, deeper than the Eutaw Formation and higher than the Washita Formation, includes three layers: the Upper Tuscaloosa Formation, the Tuscaloosa Marine shale, and the Lower Tuscaloosa Formation **(Error! Reference source not found.**-1**),** corresponding to transgression, inundation, and regression of the sedimentary process, respectively (Mancini and Puckett, 2002). The TMS was sandwiched between upper and lower Tuscaloosa sections during the Cenomanian to Turonian stages of the Upper Cretaceous, about 89-92 million years ago (Mancini and Puckett, 2002). The marine shale

occupies the extent of the sea-level rise, and sediments were accumulated by wave action. The TMS was deposited within open marine and middle to distal shelf environments (Allen et al., 2014). This is a possible reason why the total organic carbon content of TMS is similar to that of Eagle Ford Shale, which is assessed to hold approximately 3.4 billion barrels of oil (EIA., 2021). The total area of the TMS is about 7.4 million acres. The buried depth is between 10,500 ft and 14,000 ft, and the average thickness is between 230 ft and 500 ft. Oil and gas production have been found from sandstone reservoirs of the Lower Tuscaloosa in Mississippi, Louisiana, and Alabama (Allen et al., 2014; Ambrose et al., 2015), while TMS was believed as the source bed for the Lower Tuscaloosa sands (John et al., 1997). In 1950, in Mississippi, petroleum companies reported that a large amount of oil and gas had moved from the abnormal pressure zone in TMS (Nippes, 2019). The TMS has interconnected fractures and overpressure, which are probably caused by pressure increases from oil and gas generation.

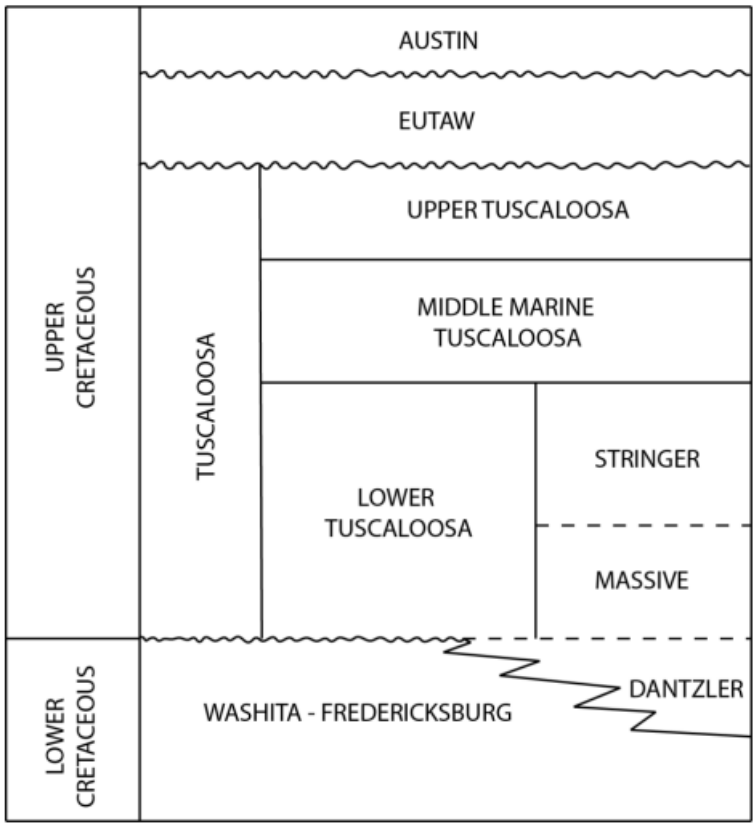

Figure 1-1: Geological map of Tuscaloosa formation (Rutherford, 1988)

The TMS has attracted adventurous investment and drilling companies, despite the potential drilling risks. Well #1 Spinks was drilled and fractured with 30,000 lbs of sand by Sun Oil Company in Pike Country, Mississippi in 1971. However, it was plugged and abandoned because of uneconomic production (Lu et al., 2015; John et al., 1997). Three years later, the well Callon #1 Cutrer was also abandoned when the running-liner job through TMS was done in Tangipahoa Parish, Louisiana. The exploration well of TMS was not successful until 1975 in Tangipahoa Parish, Louisiana (John et al., 2005). The Callon #2 Cutrer was fractured by using 80,000 lbs of sand and, in total, produced 2,500 barrels of shale oil from Tuscaloosa Marine Shale Formation between 11,073 and 11,644 ft before 1991(John et al., 1997; Nippes, 2019). The Texas Pacific #1 Blades Well in Tangipahoa Parish, Louisiana in 1977, has

produced more than 27,500 barrels of shale oil. In addition, it still produces a modest amount of oil even now.

Some vertical exploration wells of TMS failed to show good commercial performance, which reduced the interest of capital and drilling companies in TMS. John et al. (1997) presented that the TMS has an unproven estimated 7 billion barrels of recoverable production within approximately 5,900 square miles. They estimated the average thickness of TMS was between 230 and 500 ft, while the thickest area of TMS was over 800 ft in southeastern Louisiana. Resistivity measurements are useful in identifying possibly profitable deposits. The resistivity zone of above five ohms was between the surface and 325 ft. In southwestern Mississippi, the high-resistivity zone corresponds to the high proportion of Type II total organic content, which is a determining factor in a rock's ability to generate oil and gas.

The horizontal drilling technique has been used in exploration wells in TMS. The well, UPR #5 Richland Plantation, was the first directional well with an effective horizontal lateral length of 1,100 ft. Average initial production was 117 barrels of shale oil per day and a total of 3,456 barrels of shale oil in the first three months. The Worldwide #1 Braswell 24-12 Well in Mississippi, with an effective horizontal lateral length of 1,419 ft, was the first horizontal well in TMS. This well has produced shale oil production until today, a total of more than 12,700 barrels. The Encore company drilled a long horizontal section well and did single-stage stimulations in 2000; however, these attempts cannot avoid complex completion problems.

The TMS received more attention from investors and petroleum companies after the horizontal well Weyerhaeuser 73 H in the Saint Helena Parish, Louisiana produced oil at a commercial rate. The well had a horizontal length of 6,117 ft and was fractured in 17 stages with 4,255,040 lbs of proppant. In the first month, there were 18,036 barrels of oil and 7,445 thousand standard cubic feet of gas produced in total. This monthly production record showed horizontal drilling and hydraulic fracturing played key roles in production stimulation in TMS. Based on the success of Weyerhaeuser 73 H and driven by high oil and gas prices, the quick-developing period of TMS came. Between 2011 and 2015, over 80 wells of TMS were drilled using horizontal drilling and multi-stage hydraulic fracturing techniques (Durham, 2013; Durham, 2014). Unfortunately, because of the sudden drop in oil prices in 2015, the drilling activities were reduced in the summer of 2015 (Durham, 2015). The dominant TMS operator, Encana, transferred its shares to another company, Australis, and the latter drilled a few new wells.

To date, some progress in research has been made on TMS. Macroscopically, anisotropy and heterogeneity are two significant characteristics like most unconventional shale reservoirs, caused by variations in the content of the minerals. The average mineral composition of TMS-producing formation is 1.65 wt% TOC, 22.8 wt% quartz, 17.2 wt% calcite, 16.2 wt% kaolinite, 14.1 wt% illite, 11.8 wt% smectite, 5.7 wt% chlorite, 3.9 wt% plagioclase, and 4.4 wt% pyrite. (Borrok et al., 2019).

1.1.2 Effect of Temperature on Oil Viscosity

Regarding the research on the relationship between reservoir temperature and viscosity, many viscosity correlations have been developed since 1947.

The Standing correlation uses formation temperature, gas-oil ratio, and oil gravity to calculate the bubble-point pressure and oil formation volume factor. For estimating black oil properties in California, United States, the average relative error of this correlation method is less than 4.8%. The limitation of this method is that non-hydrocarbon components are not considered in this calculation model (Standing, 1947).

The Glaso correlation was derived from laboratory samples which were from North Sea oils. The correlation is suitable for the oil and gas mixture samples with nonhydrocarbons (like CO2, N2, and H2S) and paraffinicity of the oil. However, the correlation cannot be applied in differential separation data (Glaso, 1980).

The Beggs and Robinson correlation is easy to use since it does not consider the compositions of the oil, which are difficult to obtain. Therefore, the accuracy of this correlation is in an acceptable range (Beggs and Robinson, 1975).

The correlations of De Ghetto et al. are applied to determine the dead-oil viscosity, gas-saturated oil viscosity, and undersaturated oil viscosity. These correlations filled the gap that no correlations were available for extra-heavy oils. The reliability was validated by using 1200 data points of 65 heavy or extra-heavy samples (De Ghetto et al.,1995).
Based on the correlations above, oil viscosity has a non-linear negative relation with temperature (Babar et al., 2019; Nadooshan et al.2018).

Oil viscosity plays an essential role in the flow in the porous medium and wellbore, which seriously affects the transport of oil in reservoirs and the productivity of petroleum products. An inaccurate evaluation of oil viscosity leads to an unsuitable well-completion design; therefore, it results in oil reduction or excessive engineering and maintenance costs (Moller et al.,2018).

Engineers and researchers obtain crude oil viscosity from the empirical model in the field. However, the viscosity of crude oil varies from one reservoir to another due to the pressure, temperature, saturation, and so on. The empirical model of viscosity from one reservoir on the Gulf Coast has had good performance when applied to the reservoir in Bohai Sea, China. The laboratory testing is another way to obtain the viscosity of crude oil. However, it is difficult to prepare for the test since it is hard to re-generate the formation conditions and the formation oil phase states in the lab.

In the past two decades, numerical simulation has been a popular method for researchers to calculate the viscosity of crude oil, because it is fast and widely used (Li, 2019). Li (2019) simulated the gas injection process in a porous medium done to reduce the viscosity of heavy oil. The viscosity change caused by gas injection leads to the production rate increasing by a factor of 50. According to the production prediction model of Penmatcha et al. (1999), in a horizontal section of 5000 ft, the production rate of oil reduces to 2000 STB/day if the viscosity increases from 1 cp to 10 cp (Penmatcha et al.,1999). In general, the viscosity as a key parameter of oil production is heterogeneous, which makes estimating the production rate a difficult problem (Gates et al.,2008). Therefore, accurate obtaining of oil viscosity is

the key to understanding oil transport in reservoirs, optimizing the well-completion design, and then increasing the oil production. (Moller et al.,2018).

1.2 Statement of Problem

The United States Energy Information Administration (U.S.EIA) released the Annual Energy Outlook in March 2022, which gives the energy production and consumption history and projections. It shows the dry natural gas production increased and will increase from 1990 to 2050, while production of crude oil and condensate would have slight decreases before 2008 and then increase quickly in the following 13 years, and according to the projection before 2050, its production will keep at a high level, as shown in Figure 1-2 (U.S.EIA, 2022). In the energy consumption by fuel AEO2022 reference case, although the consumption of renewable energy increases and will keep increasing at a high rate, it still has a long way to go before replacing petroleum and natural gas in U.S. energy consumption. In other words, in the next 30 years, the use of petroleum and natural gas will still be indispensable in the United States.

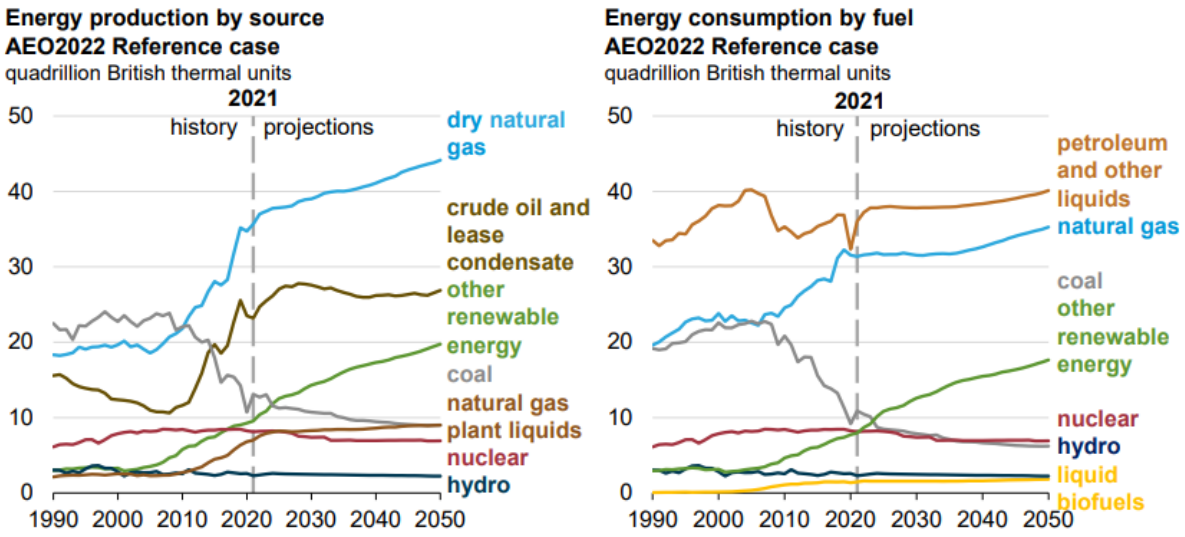

Figure 1-2: U. S. energy production and consumption forecast (U.S EIA, 2022)

As shown in Figure 1-3, U.S. crude oil production increases to 12 million b/d in the second half of 2022, which is 0.76 million b/d more than the crude oil production of 2021 (U.S. EIA, 2022). Without considering production from the Federal Offshore Gulf of Mexico and Alaska, more than 80% of crude oil production growth will come from the Lower 48 states (U.S. EIA, 2022).

In the recent 20 years, driven by economic growth and benefited from the development of new engineering technologies, especially horizontal drilling and hydraulic fracturing technologies, the development of shale oil and gas provided over 50% of the total U.S. crude oil production (U.S. EIA, 2020). The three major shale plays - Bakken Shale, Permian Shale Basin, and Eagle Ford Shale – produce 85% of non-traditional sources of oil in the United States.

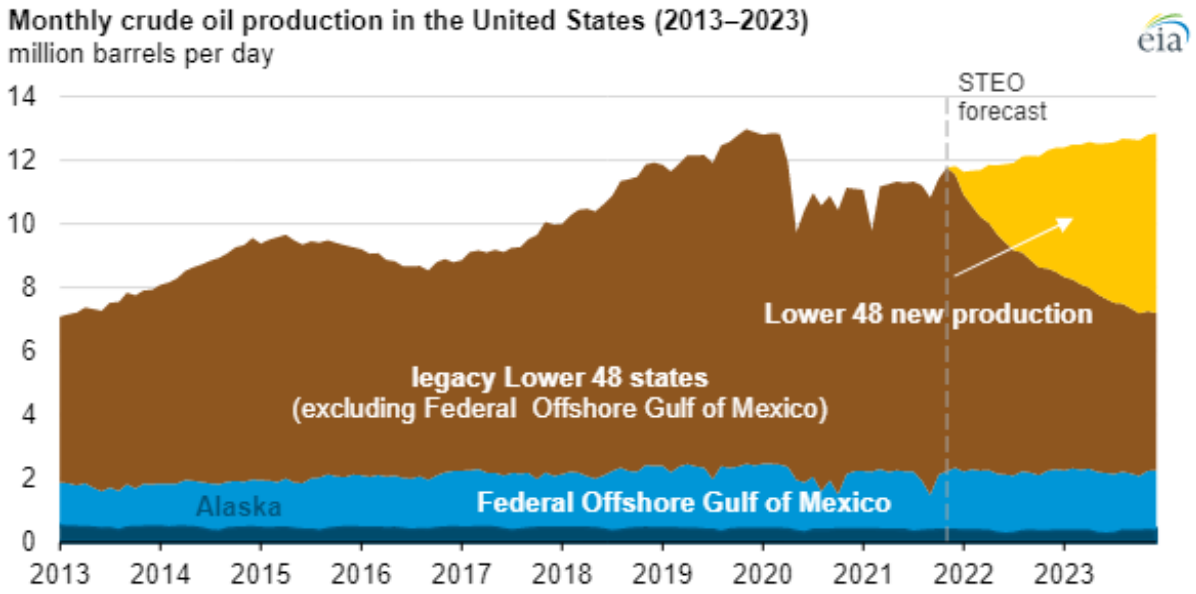

Figure 1-3: U.S. crude oil production short-term forecast (U.S. EIA, 2022)

To solve the new energy demands, developing new shale reservoirs will play a huge role in the future. Tuscaloosa Marine Shale (TMS), located across Louisiana and Mississippi, has a big potential for commercial production. As shown in Figure 1-4, The Tuscaloosa Marine Shale play refers to 22 parishes in central Louisiana and 6 counties in southern Mississippi. Although TMS is considered one of the prospective shale plays in the lower 48 states, it owns a huge advantage over other prospective shale plays since TMS is similar to Eagle Ford shale in Texas geologically. However, the TMS has higher clay/silt content than Eagle Ford shale. The TMS is the marine sedimentary layer between Upper Tuscaloosa Formation and Lower Tuscaloosa Formation in Upper Cretaceous (John et al.1997). John et al. (1997) believed the TMS held an unproven recoverable oil of seven billion barrels.

Driven by the increase in crude oil price and the improvement of drilling technologies, the drilling companies and oil companies started to extract hydrocarbon from TMS, with the

expectation of unlocking the next “Eagle Ford Shale” during 2011 - 2015. The success of Weyerhaeuser 73H Well in the Saint Helena Parish attracted much attention since it produced 18,036 barrels of oil and 7,445,000 cubic feet of gas in the first month. In 2014, at most, 18 drilling rigs worked on TMS at the same time for oil and gas production. During 2011 - 2015, encouraged by the success of Weyerhaeuser 73H Well, companies drilled more than 80 wells in TMS. By using horizontal drilling and multi-stage fracturing, some wells got substantial commercial initial production. The highest initial production was from the Richland Plantation #1 Well, 323 barrels of oil per day (Barrell, 2013). The horizontal drilling and hydraulic fracturing technologies solved the problem of low initial production.

After solving the problem of low initial production, the next problem that was urgently needed to be solved was how to increase and optimize the long-term production rate in TMS wells. However, the drilling activities were slowed down in the summer of 2015 due to the low crude oil price and high drilling cost. To reduce the cost and keep developing TMS, an innovative stimulation method is needed to optimize the long-term production rate. In this research, we investigate y-shaped well couples to transfer geothermal energy to stimulate the TMS reservoirs to increase oil production for the long term.

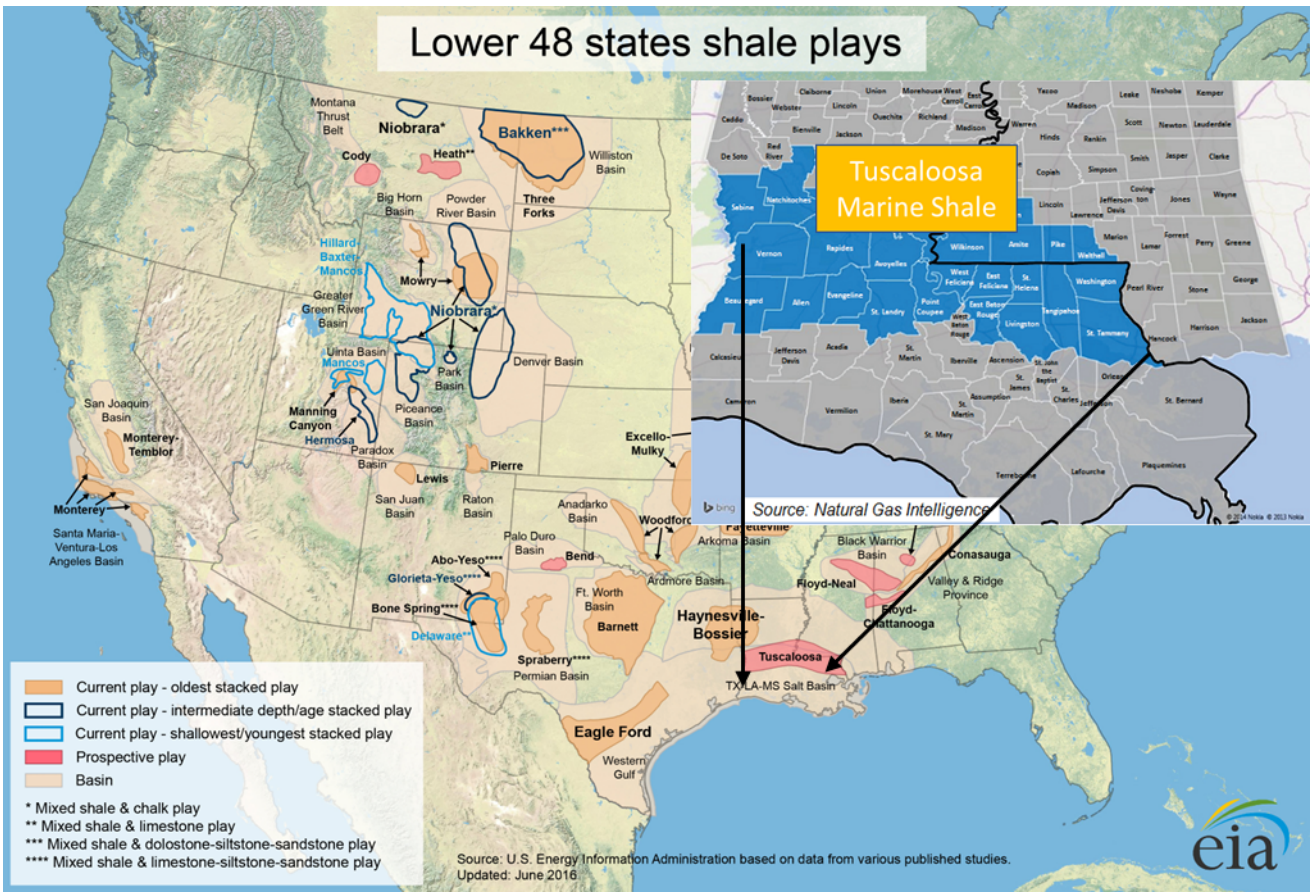

Figure 1-4: Map of U.S. Shale plays and TMS (U.S. EIA, 2022; NGI, 2022)

1. Emphasize our research contribution/ originality for this study.

In this research, we applied the geothermal energy to heat the TMS reservoir through the y-shaped well couples, to decrease the viscosity of shale oil, therefore it will increase the shale oil production rate. In this study, we used the inter-wellbore heat transfer model, the in-reservoir heat transfer model, as well as the production rate model of fractured horizontal wells, to determine the stimulated production rate of the TMS reservoir, furthermore, we did sensitivity analysis on the factors that had impact on the TMS production rate. We also proposed an analytical model to fill the gap of geothermal energy transfer in TMS reservoir and verified the model by using numerical simulation.

1.3 Research Goal and Objectives

A lot of literature points out the same key problem, i.e., the TMS has poor production performance but it has a huge potential. Research aiming at understanding of geologic characteristics of TMS and improving engineering method is a key to increasing the oil production rate of TMS wells. The overall goal of this study is to increase the well productivity in the TMS with low engineering cost by stimulating the oil reservoir with geothermal energy.

The objectives of this research are as follows:

1. Using geothermal energy to stimulate TMS well for improving well productivity.
2. Analyzing the efficiency of the geothermal stimulation method for increasing TMS reservoir temperature.
3. Determining the factors affecting the efficiency of the thermal stimulation.

These objectives are achieved through performing the following tasks:

1. Development of a mathematical model for thermal stimulation.

   This task first defines y-shaped well couples as the well trajectory for geothermal stimulation of TMS formation. Then it develops geothermal stimulation models for the defined well trajectory. Ordinary differential equations (ODE) describing the heat transfer in the y-shaped well couples are used and solutions are sought using realistic initial condition and boundary condition.

2. Analysis of heat transfer efficiency in the TMS formation.

This task aims to determine the geothermal energy transfer rate and the formation area affected by the thermal stimulation as a function of heat transfer time. A quasi-static temperature distribution is obtained by numerical simulation.

3. Prediction of well productivity improvement in the TMS formation.

An analytical model of long-term production rate is utilized to predict the effect of the well productivity in geothermal-heated reservoirs. Factors affecting the oil production rate in the stimulated TMS are identified through sensitivity analysis.

1.4 Significance of Study

The development of TMS will further enhance self-sufficiency ability of the United States with respect to oil and gas, improve its capacity to deal with oil shortages, reduce the effects of foreign conflicts on international crude oil prices, and raise oil reserves to help deal with a possible oil crisis in the future. In addition, the development of TMS will provide technical experience and engineering skills for shale oil exploitation for future shale development in the United States. Enhanced crude oil production will bring profits to the U.S. industry that can benefit many other sectors of the United States. Moreover, the application of geothermal energy should help provide a clean, environment-friendly path to producing shale oil.

1.5 Six Sigma Approach to Research Process

Six Sigma, introduced by Bill Smith of Motorola in 1986, is a systematic method with a set of management techniques and tools for process improvement. The key of Six Sigma is

called DMAIC, which includes five phases: Define, Measure, Analyze, Improve, and Control. The DMAIC is used for stabilizing, improving, and optimizing business processes and system optimization. This dissertation is organized by using the DMAIC framework of Six Sigma (Figure 1-5).

In the Define phase, the research problem, improvement activities, opportunities for improvement, the project goals, and boundaries are clearly defined. The scope of this project is to improve the oil productivity in the TMS. Opportunity for improvement refers to finding the previous research gap by doing a literature review. Improvement activities are defined as my methodology to solve this problem. The boundaries include solving this problem in the only engineering field, the location, and depth of TMS reservoir, while initial conditions are the current production status and geothermal distribution of reservoir and formations. The Define phase corresponds to the previous research and the current research problem in Chapter 1 of this dissertation.

The mathematical modeling of oil production corresponds to the Measure phase. The developed mathematical modeling is the way to process the collected data from TMS reservoirs. The purpose of the Measure phase is to compare the production rate of TMS to a similar shale like Eagle Ford shale, which shows the current performance of TMS.

The determination of the relationship between shale oil production and geothermal energy corresponds to the Analyze phase. The purpose of the Analyze phase is to determine the

parameters, which affect shale oil production. In this phase, I am going to determine the root causes of the production issues. The key point of Analyze phase is to verify hypotheses before implementing solutions.

The methodology of the y-shaped well corresponds to the Improve and Control phases. When the root causes are determined in the Analyze phase, the solution should be used to resolve the root causes. In this phase, the TMS data are used to obtain measurable improvement by using an innovative oil well stimulation methodology and then comparing it to the current production result. In the Control phase, the process is monitored and further optimization is attempted.

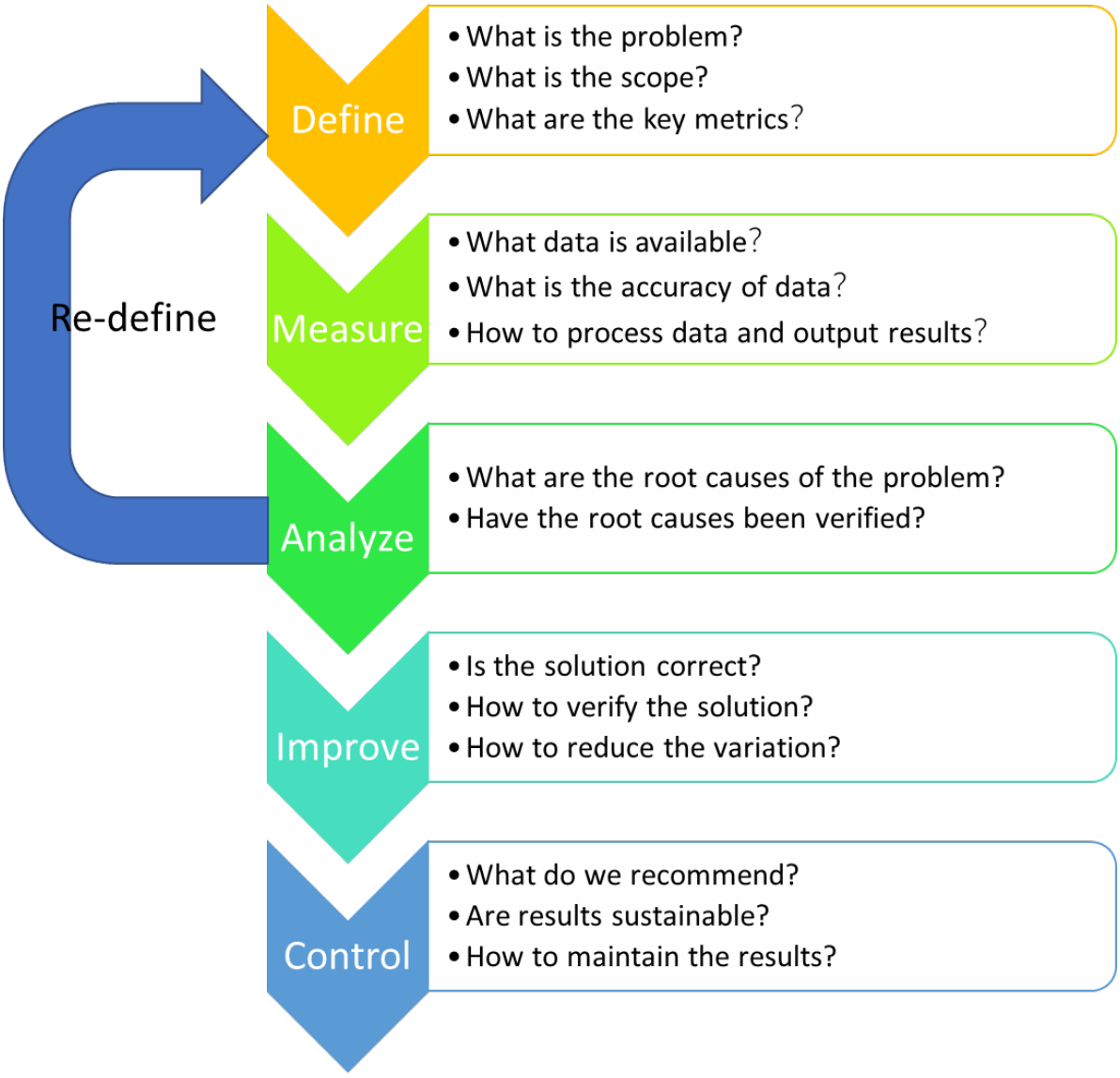

Figure 1-5: The DMAIC flow chart

Chapter 2: Heat Transfer Models

2.1 System Description

Fu et al. (2021) proposed an innovative system called y-shaped well couple to transfer heat from a geothermal zone to a hydrocarbon pay zone (Figure 2-1). The system involves three horizontal wellbore sections. From top to bottom, the first and second horizontal wellbores are heat dissipator and hydrocarbon producer, respectively. Both are drilled through a hydrocarbon-bearing zone. The third horizontal wellbore is the heat absorber that is drilled through the geothermal zone. The work fluid continuously injected into the water injector serves as a medium for transferring heat from the geothermal zone to the hydrocarbon-bearing zone. The geothermal energy around the heat absorber wellbore heats the work fluid as it flows through the annular space of the wellbore. The heated fluid flows back up the annulus and into the first horizontal wellbore, heating the hydrocarbon-bearing zone and lowering oil viscosity. The heated oil is produced through the oil producer wellbore. The returned work fluid is recycled along the path indicated by the arrows.

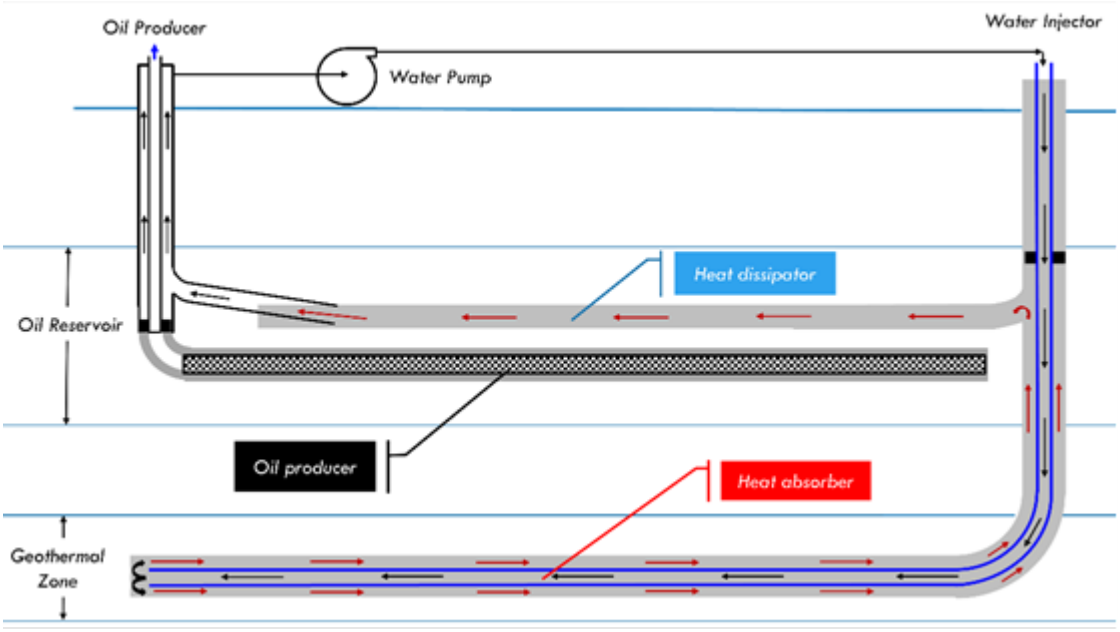

Figure 2-1: Schematic diagram of a y-shaped well couple for heat transfer from a geothermal zone to a TMS reservoir (modified from Fu et al., 2021)

2.2 Mathematical Model for Inter-Wellbore Heat Transfer

Fu et al. (2021) presented a mathematical model of the heat transfer in a y-shaped well couple with simplified wellbore segments namely Sections I, II, III, and IV as shown in Figure 2-2. While the initial mathematical model for gas hydrate reservoirs was described in Fu et al.'s (2021) paper and modified derivation for shale oil reservoirs is shown in Appendix A, resultant equations are reviewed here.

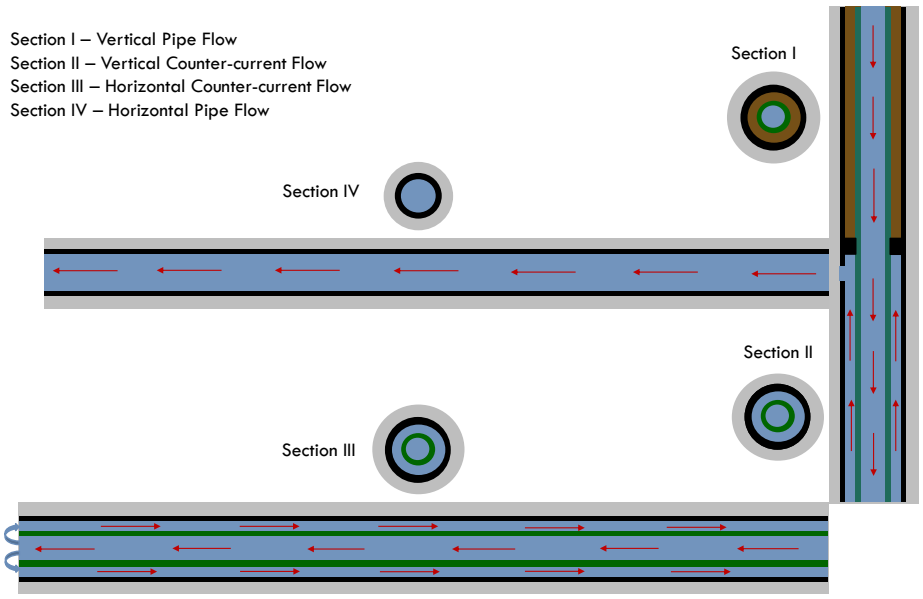

Figure 2-2: Wellbore segments in a Y-shaped well couple (Fu et al., 2021)

The temperature profile in Section I:

$$T_p = \frac{1}{\alpha_{p1}^2}[\beta - \alpha_{p1}\beta L - a_{p1}\gamma + e^{-\alpha_{p1}(L+C)}] \quad (2\text{-}1)$$

where L is the length of the section in m, and

$$\alpha_{p1} = \frac{\pi D_p K_a}{C_p \dot{m}_p t_a} \quad (2\text{-}2)$$

$$\beta = -\alpha_{p1} G \quad (2\text{-}3)$$

$$\gamma = -\alpha_{p1} T_{g0} \quad (2\text{-}4)$$

$$C = -\frac{1}{\alpha_{p1}} \ln [-\beta + \alpha_{p1}^2 T_{p0} + \alpha_{p1}\gamma] \quad (2\text{-}5)$$

where T_p is fluid temperature in the pipe at target depth in ºC, D_p is the outer diameter of work pipe in m, K_a is the thermal conductivity of annulus fluid in W/m-ºC, C_p is the heat capacity of the work fluid in J/kg-ºCJ/kg℃, $\dot{m}_p$ is the mass flow rate of work fluid in kg/s, is, t_a is the thickness of annulus in m, G is the geothermal temperature gradient, T_{g0} is the geothermal temperature at surface in ◦C.

The temperature profile in Section II:

$$T_p = C_1' A' e^{r_1 L} + C_2' A' e^{r_2 L} + a'L + \frac{A'a' + A'B'b' - a'(B' + E')}{A'B'} \quad (2\text{-}6)$$

$$T_a = C_1'(A' + R_1)e^{R_1 L} + C_2'(A' + R_2)e^{R_2 L} + a'L + \frac{A'a' + A'B'b' - a'E'}{A'B'} \quad (2\text{-}7)$$

where,

$$C_1' = \frac{A'B'(A'D' - a') - [A'B'C' - A'B'b' - A'a' + a'(B' + E')]R_2 e^{R_2 L_2}}{A'2B'(R_1 e^{R_1 L_2} - R_2 e^{R_2 L_2})} \quad (2\text{-}8)$$

$$C_2' = \frac{-A'B'(A'D' - a') - [A'B'C' - A'B'b' - A'a' + a'(B' + E')]R_1 e^{R_1 L_2}}{A'2B'(R_1 e^{R_1 L_2} - R_2 e^{R_2 L_2})} \quad (2\text{-}9)$$

$$R_1 = \frac{B' + E' - A' + \sqrt{(B' + E' - A')^2 + 4A'B'}}{2} \quad (2\text{-}10)$$

$$R_2 = \frac{B' + E' - A' - \sqrt{(B' + E' - A')^2 + 4A'B'}}{2} \quad (2\text{-}11)$$

where $A' = \alpha = \alpha$, $B' = \alpha$, $C' = T$, $D' = \Delta T$, $E' = \beta$, $a' = G$, and $b' = T$.

The temperature profile in Section III:

$$T_p = C_1 A e^{r_1 L} + C_2 A e^{r_2 L} + b \quad (2\text{-}12)$$

$$T_a = C_1(A + r_1)e^{r_1 L} + C_2(A + r_2)e^{r_2 L} + b \quad (2\text{-}13)$$

where T_a is fluid temperature in the annulus at target depth in ^{o}C

$$C_1 = \frac{AB(C - b)r_2 e^{r_2 L_3}}{A^2 B(r_1 e^{r_1 L_3} - r_2 e^{r_2 L_3})} \quad (2\text{-}14)$$

$$C_2 = \frac{AB(C - b)r_1 e^{r_1 L_3}}{A^2 B(r_1 e^{r_1 L_3} - r_2 e^{r_2 L_3})} \quad (2\text{-}15)$$

where,

$$r_1 = \frac{B + E - A + \sqrt{(B + E - A)^2 + 4AB}}{2} \quad (2\text{-}16)$$

$$r_2 = \frac{B + E - A - \sqrt{(B + E - A)^2 + 4AB}}{2} \quad (2\text{-}17)$$

where $A = \alpha_{p3}$, $B = \alpha_{a3}$, $C = T_{p2}$, $E = \beta_{a3}$, $b = T_{g3}$.

The temperature profile in Section IV:

$$T_p = \frac{1}{\alpha_{csg}}\left[(\alpha_{csg}T_{a1} + \gamma_{csg})e^{-\alpha_{csg}L4} - \gamma_{csg}\right] \quad (2\text{-}18)$$

where

$$\alpha_{csg} = \frac{\pi D_{csg}K_c}{C_p\dot{m}_p t_c} \quad (2\text{-}19)$$

$$\gamma_{csg} = -\alpha_{csg}T_{g4} \quad (2\text{-}20)$$

where T_{a1} is fluid temperature (℃) in the annulus of Section I below the packer, T_{g4} is the average geothermal temperature (℃) at the depth of section IV, *L4* is distance (m) from the fluid entry point (length of Section IV), D_{csg} is the outer diameter (m) of the casing in Section IV (inner diameter of cement sheath), K_c is the thermal conductivity of cement sheath in $W/m \cdot ℃$, C_p is the heat capacity of the work fluid in $J/kg \cdot ℃$, $\dot{m}_p$ is the mass flow rate of work fluid in kg/s, t_c is the thickness of cement sheath in m.

2.3 Mathematical Model for In-Reservoir Heat Transfer

This section presents a newly developed analytical model for describing the heat transfer from wellbore into the oil pay zone and a numerical model to validate the analytical model.

2.3.1 Analytical Model

Governing Equation. The governing equation of temperature is the commonly known diffusivity equation expressed as

$$\frac{1}{r}\frac{\partial}{\partial r}\left(r\frac{\partial T}{\partial r}\right)=\frac{1}{\beta}\frac{\partial T}{\partial t} \tag{2-21}$$

where T is temperature in ^{o}C, r is distance from the wellbore center line in meter, t is time in second, and b is thermal diffusivity constant defined by

$$\beta=\frac{K}{\rho_s C_{ps}} \tag{2-22}$$

where K is rock thermal conductivity in W/m-^{o}C, r_s is rock density in kg/m^3, and C_{ps} is rock heat capacity at constant pressure (specific heat) in J/kg-^{o}C.

Initial Condition. The initial condition is expressed as

$$T=T_i \quad \text{at } t=0 \text{ for all } r. \tag{2-23}$$

where T_i is the initial reservoir temperature.

Boundary Conditions. The boundary condition at the wellbore is expressed as

$$q_{r_w}=-K\left[\frac{dT}{dr}\right]_{r=r_w} \quad \text{for all } t. \tag{2-24}$$

where q_{rw} is rate of flow of heat per unit time per unit area of wellbore in J/s-m^2. For a circular wellbore with radius r_w and length L,

$$q_{r_w}=\frac{Q_{r_w}}{2\pi r_w L}$$

where Q_{rw} is rate of flow of heat per unit time in J/s. Then Eq. (2-24) and rearranging the latter gives

$$\frac{Q_{r_w}}{2\pi LK}=-r_w\left[\frac{dT}{dr}\right]_{r=r_w} \quad \text{for all } t. \tag{2-25}$$

Another boundary condition is obvious:

$\frac{r^2}{4\beta t}$ approaches to 0 as *t* increases. (2-26)

Solution. The solution of Eq. (2-21) takes the following form (see **Appendix B** for derivation):

$$T = T_i + \frac{Q_{r_w}}{4\pi LK} E_i(s) \tag{2-27}$$

where Ei(s) is the exponential integral and

$$s = \frac{r^2}{4\beta t} \tag{2-28}$$

The heat flow rate from wellbore to reservoir can be calculated by

$$Q_{rw} = C_{pl}\dot{m}_p(T_{in} - T_{out}) \tag{2-29}$$

where C_{pl} is the heat capacity of the fluid inside the wellbore in $J/(kg \cdot ℃)$, $\dot{m}_p$ is the mass flow rate inside the wellbore in kg/s, and T_{in} and T_{out} are fluid temperatures in ℃ at the inlet and outlet of the wellbore, respectively.

2.3.2 Numerical Model

A two-dimensional numerical model was built in the finite-element software COMSOL Multiphysics to verify the accuracy of Eq. (2-30). Considering the symmetry of the system, the numerical model was set up with the cylindrical coordinates (r-z coordinates) with the horizontal wellbore set in the z-direction and heat transfer in the radial r-direction. The governing equation for heat transfer is as follows

$$\rho C_{ps} \frac{\partial T}{\partial t} + \rho C_{ps}\mathbf{u} \cdot \nabla T + \nabla \cdot \mathbf{q} = \mathrm{Q} \tag{2-30}$$

where ρ is the solid density in kg/m^3, C_{ps} is the heat capacity of the solid in $J/(kg \cdot ℃)$, T is temperature in ^oC, t is the time in s, $\mathbf{u}$ is the velocity field in m/s, $\mathbf{q} = -K\nabla T,$ and Q is the heat source in W/ m^3.

Figure 2-3 shows a radial cross-section of a two-dimensional discrete grid system built in the numerical model. The formation rock was assumed to be homogeneous and isotropic. The dimensions of the domain are 10 m of height in z-direction, 400 m of outer boundary in r-direction, and 0.3 m of inner boundary in r-direction (r_w). The initial condition is given by Eq. (2-23) and the inner boundary condition is described by Eq. (2-24). The mapped mesh is applied with a minimum element size of 0.02 m and a maximum size of 0.3 m.

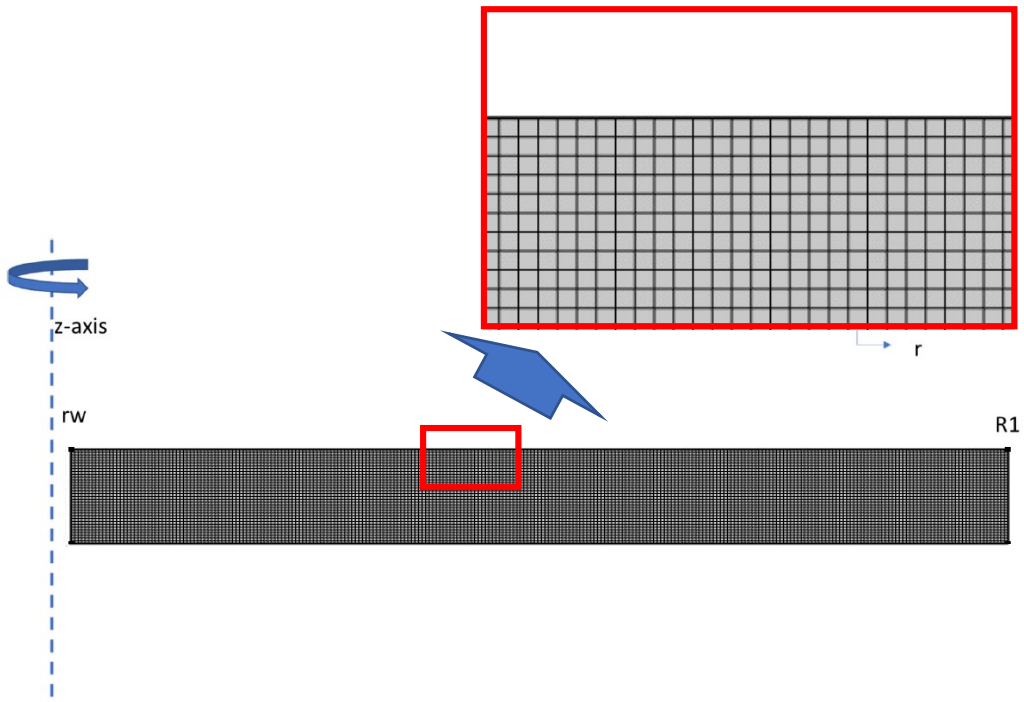

Figure 2-3: A two-dimensional discrete grid system built in the numerical model

2.3.3 Model Validation

The analytical model was validated by a comparison of its results and the results given by the numerical model for an arbitrary data set shown in Table 2-1. A comparison of temperature profiles given by the analytical and numerical models is presented in Figure 2-4. It shows the temperature rise at different radial distances from the wellbore using the data set presented in Table 2-1 in the numerical model. It indicates that the rate of temperature rise slows down with time. A comparison of results given by the numerical model and that by Eq. (2-27) was made using the same data set. A comparative plot is presented in Figure 2-5. This

comparison indicates that the results given by the two models are identical, which implies the correctness of the analytical model. Figure 2-5 presents the temperature raise at different radial distances given by the numerical model. It indicates that the rate of temperature rise diminishes with radial distance.

Table 2-1: An Input Data Set for Model Comparison

Model Parameter	Value	Unit
Solid density (ρ_s)	2,600	kg/m^3
Solid thermal conductivity (K)	1	W/m-°C
Solid heat capacity (C_{ps})	1	J/kg-°C
Solid initial temperature (T_i)	20	°C
Liquid density (ρ_L)	1000	kg/m^3
Liquid heat capacity (C_{pl})	1	J/kg-°C
Borehole length (L)	10	m
Borehole radius (r_w)	0.3	m
Liquid flow rate (Q_f)	0.01	m^3/s
Borehole inlet temperature (T_{in})	100	°C
Borehole outlet temperature (T_{out})	30	°C

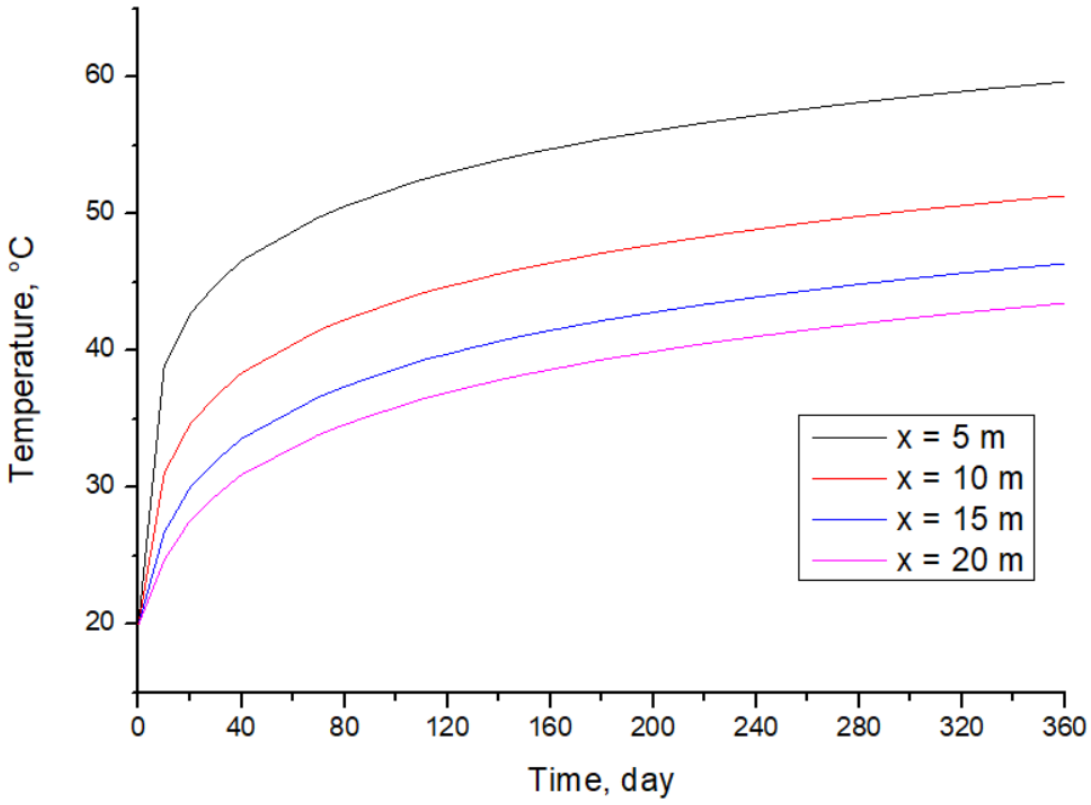

Figure 2-4: Temperature raise at different radial distances from wellbore

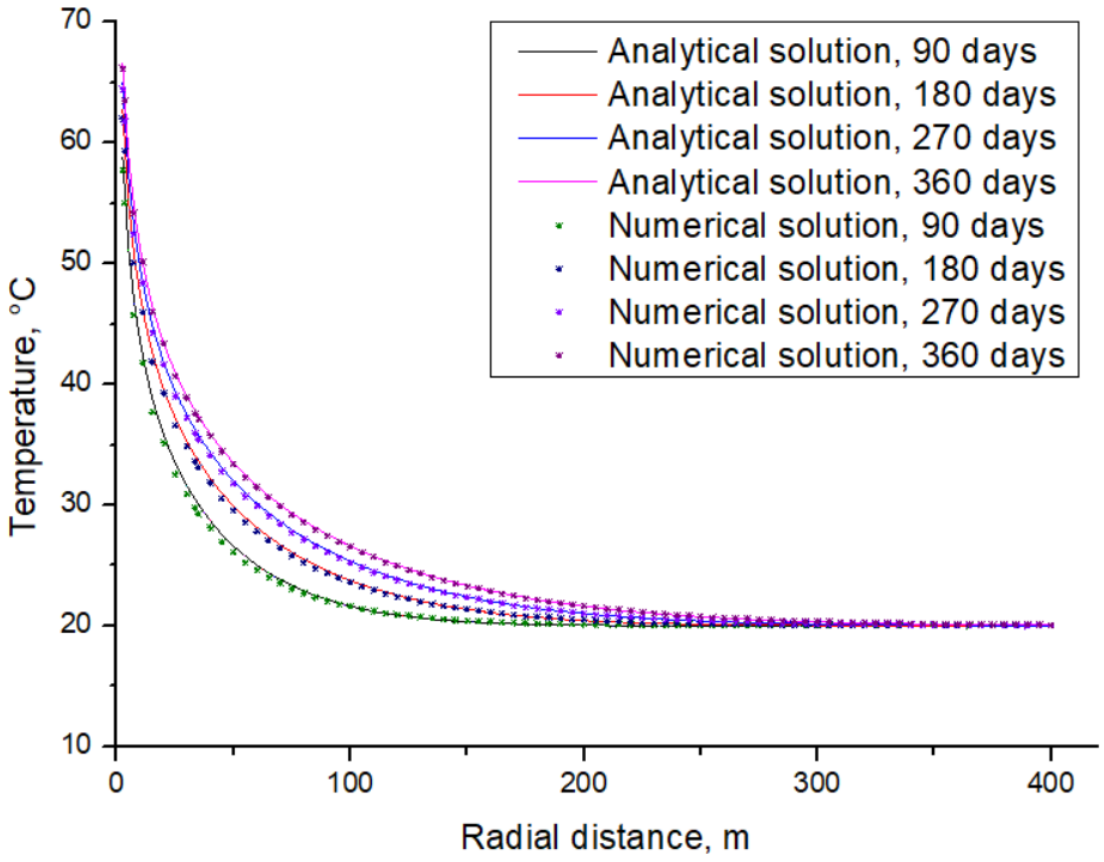

Figure 2-5: Comparison of results given by the analytical and numerical models

Chapter 3: Heat Transfer Analysis

3.1 General Temperature Profile of the Y-shaped Well

Figure 3-1 shows temperature profile along the flow direction of the work fluid in the y-shaped well. The data set used in the calculation is in Table 3-1 (Berch, 2014; Hackley and Cardott, 2016; Lohr et al., 2016; Borrok et al., 2019; Yang and Guo, 2019b). The vertical axis shows the temperature at each location of the y-shaped well, while the horizontal axis represents the traveling distance of the work fluid. The curves represent the temperature profiles in the pipe and in the annulus, respectively. The four sections of the y-shaped well are differentiated by different colors.

Table 3-1: Data Set Used in Inter-wellbore Heat Transfer Calculations

Parameter	Value	Unit
Inner diameter of work pipe	0.1038	m
Thickness of work pipe	0.005207	m
Outer diameter of work pipe	0.1143	m
Clearance of wellbore annulus	0.02588	m
Thickness of cement sheath	0.02063	m
The cross-sectional area of the annulus in Sections I, II, and III	0.01139	m^2
The inner cross-sectional area of pipe in Sections I, II, and III	0.008471	m^2
Heat capacity of fluid in the annulus in Section I	4184	$J/(kg-℃)$
Heat capacity of work fluid	4100	$J/(kg-℃)$
Thermal conductivity of annulus fluid	0.598	$J/(kg-℃)$
Thermal conductivity of pipe	45	$W/(m-℃)$
Thermal conductivity of cement in Sections I and II	0.1	$W/(m-℃)$
Thermal conductivity of cement in Sections III and IV	0.54	$W/(m-℃)$
Fluid flow rate inside work pipe	0.004-0.01	m^3/s
Geothermal temperature at surface	20	℃
The temperature of work fluid at surface	40	℃
Work fluid density	1030	kg/m^3
Length of Section I	3600	m
Length of Section II	3400	m
Length of Section III	1000	m
Length of Section IV	1900	m
Cement sheath thickness in Section IV	0.04445	m
Outer diameter pipe in Section IV	0.1143	m
Inner cross-sectional area of casing in Section IV	0.008471	m^2
Producing wellbore diameter	0.15875	m

Reservoir depth	3600	m
Thermal gradient	0.022	$℃/m$

We can see a clear upward trend of temperature when the traveling distance increases in the pipe. The slopes of the curves for Sections I and II in the pipe are the same since the geothermal gradient is constant and the temperature rise in the wellbore is caused by geothermal energy. The temperature is constant in section III, because it is in geothermal zone. From the surface to the bottom of the well, overall, the temperature increases from 40 ºC to 174 ºC.

In Section I of the well, the initial work fluid on the surface is 40 ºC, while the temperature on the surface is 20 ºC, which causes a decrease in temperature of the work fluid since it releases the heat energy. When the temperature in the formation is higher than that of the work fluid, the fluid is heated again and the temperature increases.

In Section II of the well, the low-temperature fluid that comes from the exit of Section I in the pipe is heated by the high-temperature fluid rapidly, so the temperature in the pipe increases quickly. Along the temperature profile in the pipe, the temperature difference between in the pipe and in the annulus decreases, therefore the rate of transferred energy decreases gradually, and the slope of the in-pipe temperature curves decreases to a constant value.

In Section III of the well, there is no significant temperature change between the fluid in the pipe and in the annulus. This is because Section III of the well is a horizontal line in a geothermal zone, where a sufficiently slow flow rate of the work fluid is used and thus long enough retention time for heat transfer occurred in Section III. The work fluid can reach the same temperature of the geothermal zone. The slight temperature difference in the pipe and in the anulus is neglectable.

Section IV of the well is horizontal in the TMS reservoirs, so the temperature gradient is nearly zero. The geothermal energy stored in the work fluid is released to the reservoirs in this section. Ideally, the temperature of the work fluid at the exit of Section IV drops to the geothermal temperature at the corresponding depth of the formation. Overall, the temperature profile in Section IV is the key for the energy transfer in the wellbore. It reflects the amount of energy that can be used in heating the TMS formation.

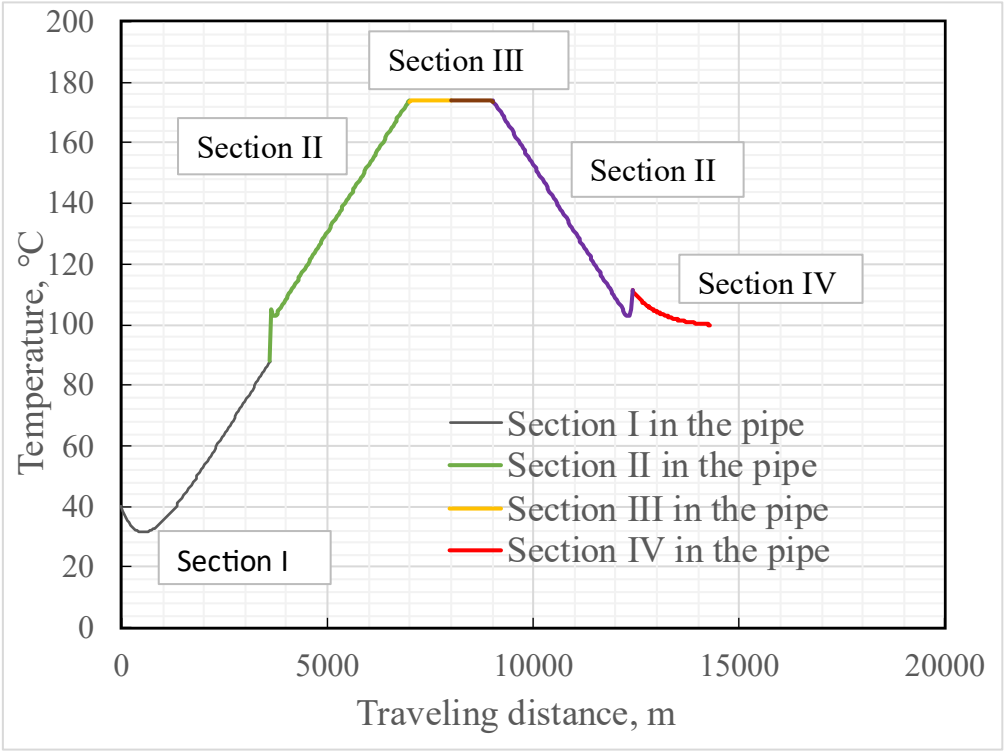

Figure 3-1: Temperature profile of the y-shaped well

3.2 Factor Affecting Wellbore Temperature Profile

It is essential to know the effects of major well parameters on the temperature profile in the y-shaped well system. These well parameters include flow rate of work fluid, oil pay zone depth, geothermal zone depth, and wellbore insulation.

3.2.1 Effect of Fluid Flow Rate

Flow rate is the easiest adjustable parameter in field applications. Figure 3-2 shows the temperature profile of Section IV at different fluid flow rates. The blue line is the geothermal temperature at the corresponding depth of the formation. Overall, the temperature from the entrance of Section IV to the exit decreases with a constant slope. With the flow rate of 0.01 m3/s, the temperature decreases from 167 ºC to 151 ºC, or a difference of 16 ºC. With the

flow rate of 0.004 m3/s, the temperature decreases from 140 ºC to 120 ºC, or a difference of 20 ºC. Comparing the temperature change at the two flow rates, the lower flow rate leads to more temperature change. However, Eq. (2-29) indicates that the heat flow rate from wellbore to reservoir depends on not only temperature drop but also flow rate. In this case, the ratio of flow is 0.004/0.01 = 0.4, while the ratio of temperature increase is 20/16 = 1.25. The resultant ratio in heat flow rate is (0.4) (1.25) = 0.5. Therefore, reducing flow rate results in a 50% drop in heat flow rate in this case. Nevertheless, this should not be considered as a general conclusion because there may be conditions where the temperature change is a dominating factor affecting the heat transfer rate. The influencing factor could be the length of Section IV wellbore that affects the retention time of fluid in the wellbore for heat transfer.

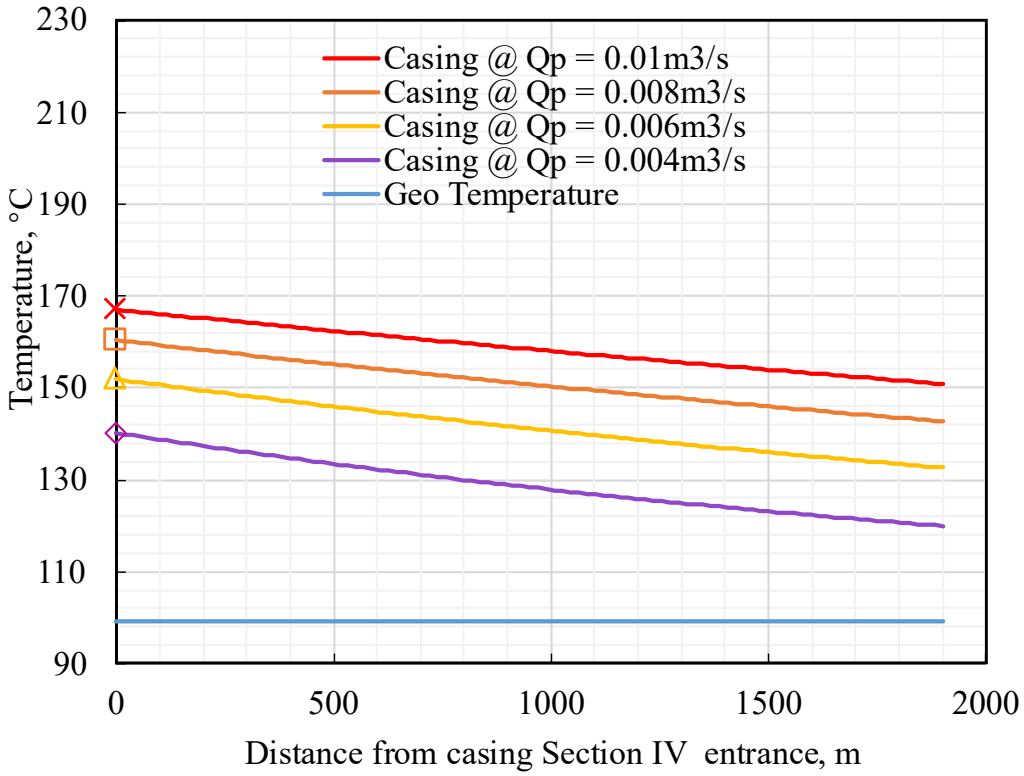

Figure 3-2: Temperature profile of Section IV at different flow rate

3.2.2 Effect of Oil Pay Zone Depth

The temperature of fluid and thus heat energy delivered to the Section IV wellbore depends on the depth of the pay zone (length of Section I). The oil pay zone depth varies from 2,600m to 4,600m in TMS. Figure 3-3 shows the effect of different lengths of Section I on the temperature profile in the pipe across the whole y-shaped well. Overall, the basic shapes of the temperature profiles in the pipes with different lengths of Section I are the same. In Section I, the temperature increases approaching the geothermal gradient. In Section II, the temperature rapidly increases about 8 ºC above the value at the end of Section I in the pipe, and then the temperature goes up following the geothermal gradient. The temperatures in Section III in the pipe and in the annulus are constant. In Section IV, the temperature drops

slowly to the oil reservoir temperature Comparing the temperatures in Section IV for different lengths of Section I, about 22 ºC temperature increase is expected in the Section IV for all cases. However, this temperature increase should increase well productivity more in shallow oil reservoir compared to deep reservoirs. The temperature effects on oil viscosity and thus well productivity are discussed in latter sections.

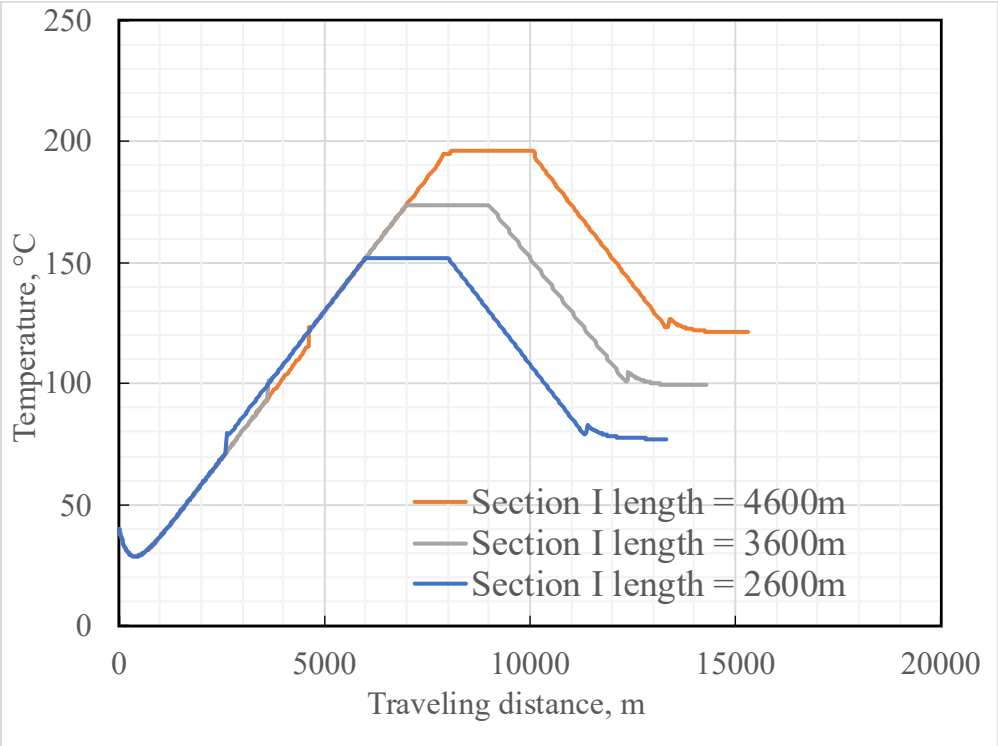

Figure 3-3: Temperature profile of the well for different lengths of Section I wellbore

3.2.3 Effect of Geothermal Zone Depth

The depth of geothermal zone is equal to the depth of oil pay zone (Section I) plus the length of Section II. For a given depth of oil pay zone, Section II is varied from 3400 m to 7000 m in this case study. Figure 3-5 shows the effect of length of Section II on the temperature

profile in the Section IV. It is seen that the temperature profiles in Section IV for different lengths of Section II are essentially the same. The temperature profile in Section IV is not sensitive to the length of Section II. This may be attributed to the heat loss in Section II.

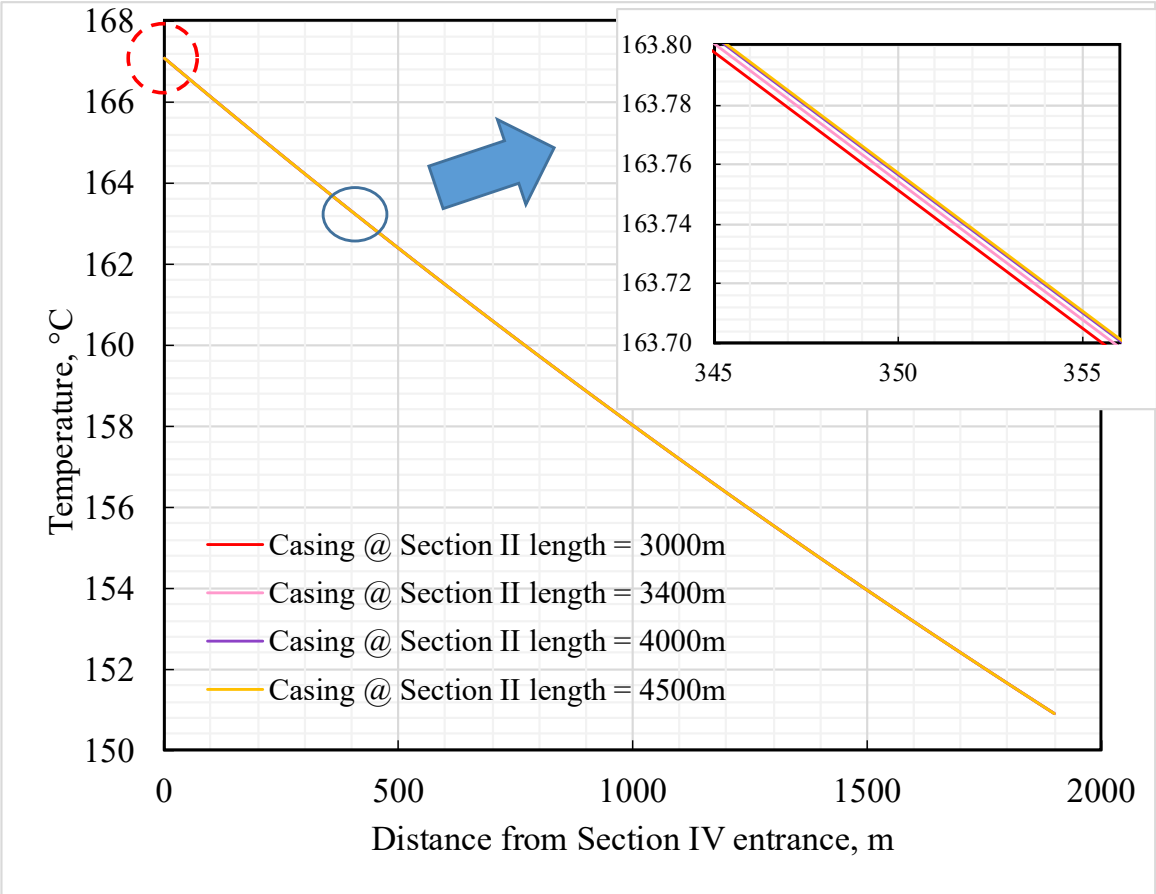

Figure 3-4: Temperature profile in Section IV with different Section II lengths

3.2.4 Effect of Wellbore Insulation

The results of the analyses presented in the previous section show that the temperature gradients in Section II are essentially equal to the geothermal gradient. Therefore, the fluid temperature delivered to the Section IV does not vary with the length of Section II. This is attributed to the heat loss across the cement sheath in Section II. If the thermal conductivity of

the cement sheath can be reduced, or an insulation layer is applied to the casing surface, the delivered temperature can be increase. Unfortunately, the analytical heat transfer model for the Section II does not consider the thermal conductivity of cement sheath. To simulate the effect of insulation on the deliverable temperature to Section IV, the thermal conductivity (K_a) of annulus fluid in the Section II is altered and investigated. The result is shown in Figure 3-5. The curves in the figure clearly indicate that the fluid temperature delivered to the oil reservoir can be increased using low-thermal conductivity materials in the heat transfer wellbore (Section II). Therefore, it is a good practice to use either low-thermal conductivity cement sheath or an insulation layer applied to the casing surface.

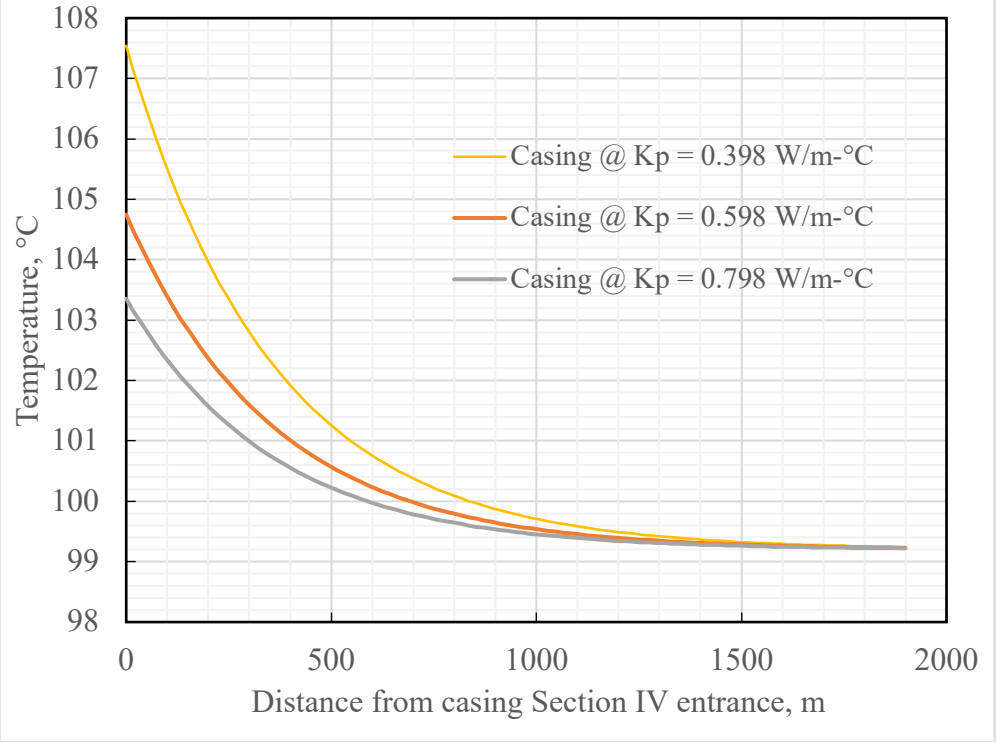

Figure 3-5: Temperature profile in Section IV for different thermal conductivity of annular fluid in section II

3.3 Factors Affecting the Temperature Inside the Oil Pay Zone

Heat transfer from the geothermal zone to the Section IV wellbore is only the first step in applying geothermal energy to develop a shale formation. The second step is the heat transfer

from Section IV into the reservoir. We performed sensitivity analysis of heat transfer by changing the formation parameters that have uncertainties in determination. We assume that a constant supply of energy from the wellbore Section IV. There are three varying parameters considered: the heat capacity of the rock, the thermal conductivity of the rock, and the density of the rock. Parameter values used in the calculation of heat transfer in the reservoir are presented in Table 3-2 (Berch, 2014; Hackley and Cardott, 2016; Lohr et al., 2016; Borrok et al., 2019; Yang and Guo, 2019b).

Table 3-2: TMS Data Used in In-reservoir Heat Transfer Calculations

Model Parameter	Value	Unit
Shale density (r_s)	2,430	kg/m^3
Shale thermal conductivity (K)	2.5	W/m-C
Shale heat capacity (C_{ps})	1500	J/kg-C
Solid initial temperature (T_i)	99.2	C
Liquid density (r_L)	1000	kg/m^3
Liquid heat capacity (C_{pl})	4200	J/kg-C
Borehole length (L)	10	m
Borehole radius (r_w)	0.3	m
Liquid flow rate (Q_f)	0.01	m^3/s
Borehole inlet temperature (T_{in})	104.7	C
Borehole outlet temperature (T_{out})	99.2	C

3.3.1 Heat Capacity of the Rock

Heat capacity represents the amount of energy needed to increase temperature by 1 ºC for 1 kg of material. Heat transfer in the reservoir is a time-dependent process and thus the temperature is a function of time.

Figure 3-6 shows the temperature profile in the near-wellbore formation for different heat capacities of the rock at the end of 360 days of heat transfer. The horizontal axis presents the radial distance from the wellbore and the vertical axis shows the temperature at distance. Overall, a significant increase in the temperature within a 10-meter distance away from the wellbore is predicted by the mathematical model. This increase in temperature depends slightly on the heat capacity of the rock. The heating will cause higher temperature rise in lower heat capacity rocks than in higher heat capacity rocks. This is expected because more energy is required to heat the high-heat capacity materials than that to heat low-heat capacity materials to the same temperature.

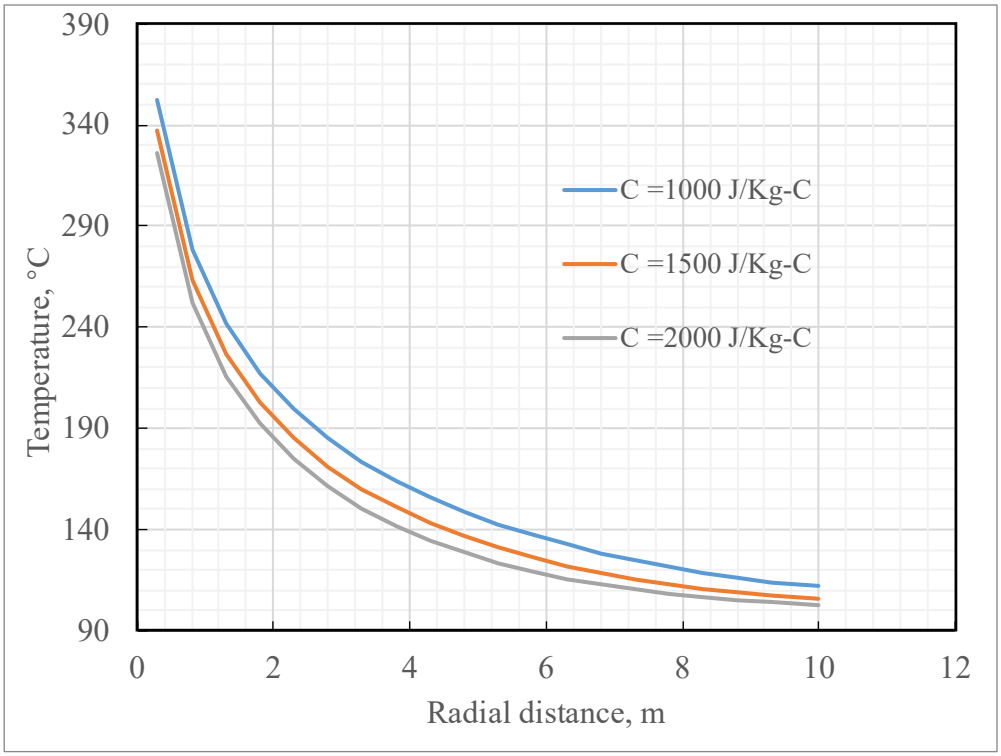

Figure 3-6: Temperature profile in the reservoir with different rock heat capacities (360 days)

3.3.2 Thermal Conductivity of the Rock

The thermal conduction is defined as the transport of energy due to random molecular motion across a temperature gradient. The thermal conductivity of the rock is a measure of the rock's ability to conduct heat. Figure 3-7 presents calculated temperature profile in the near-wellbore formation of three different thermal conductivities at the end of 360 days of heat transfer. The horizontal axis presents the radial distance from the wellbore and the vertical axis shows the temperature at distance. A significant increase in the temperature within a 5-meter distance away from the wellbore is predicted by the mathematical model. This increase in temperature strongly depends on the thermal conductivity of the rock. The trends of the three curves are consistent with the common sense in that the heat transfers faster laterally in high-thermal conductivity rocks than in low-thermal conductivity rocks. Therefore, shales with higher water saturations are better candidates for thermal stimulation than that with low water saturations because water increases rock's overall thermal conductivity.

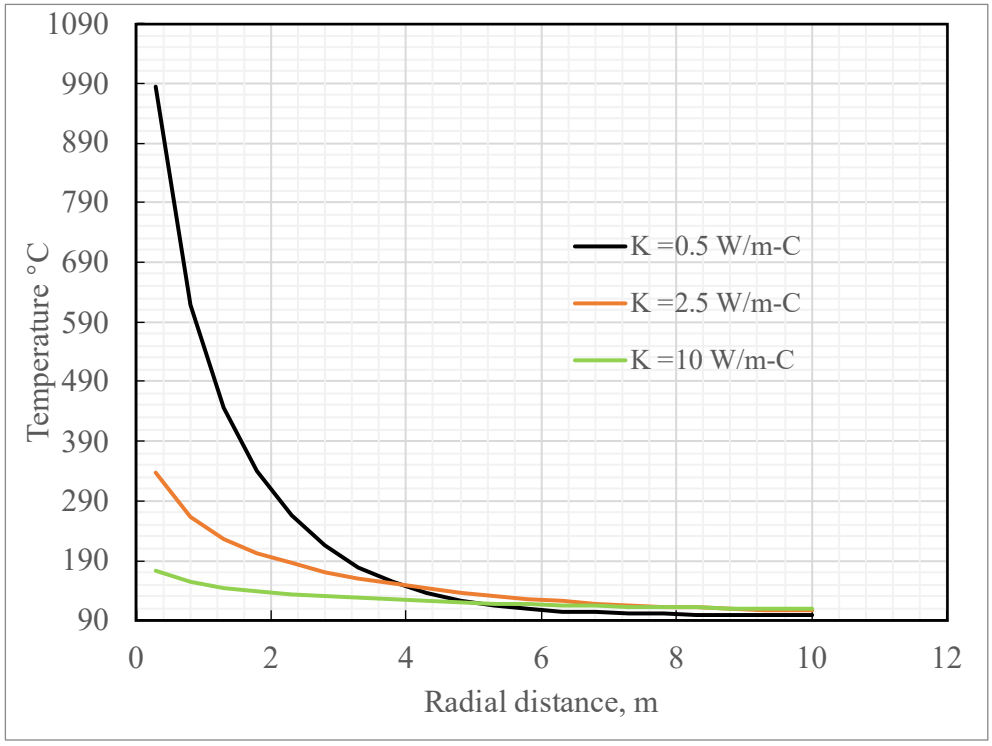

Figure 3-7: Temperature profile within the reservoir for different rock thermal conductivities (360 days)

3.3.3 Density of the Rock

Density is defined as the amount of mass in unit volume of material. Figure 3-8 shows calculated temperature profile in the near-wellbore formation of three different densities at the end of 360 days of heat transfer. The horizontal axis presents the radial distance from the wellbore and the vertical axis presents the temperature at the distance. A significant increase in the temperature within a 10-meter distance away from the wellbore is predicted by the mathematical model. This increase in temperature slightly depends on the density of the rock. The temperature increase at a given distance is higher in low-density racks than that is high-density rocks. This is expected because the same amount of heat energy can heat up more volume of low-density rock than that of high-density rock to the same temperature.

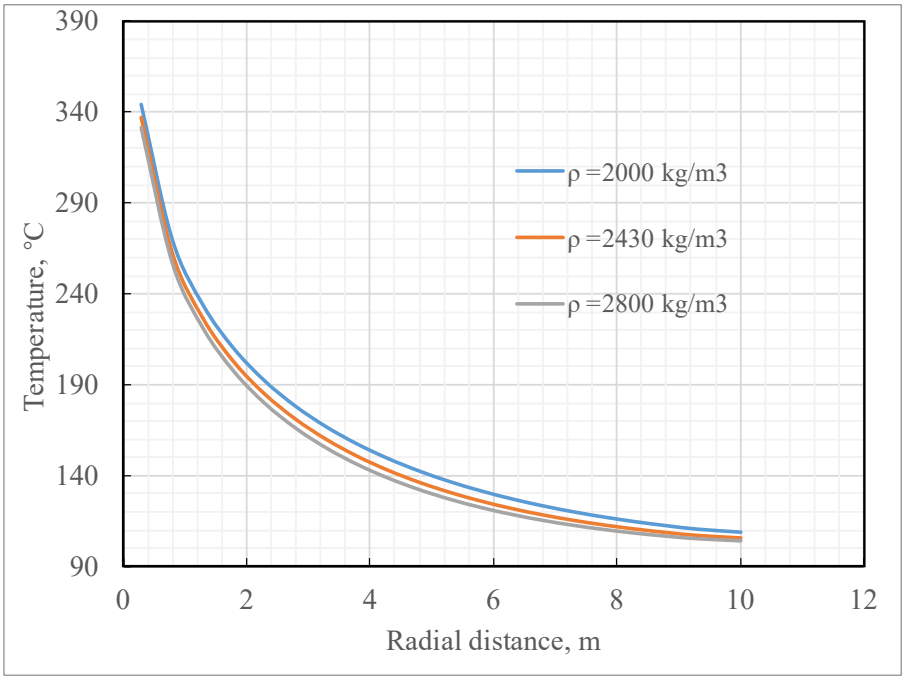

Figure 3-8: Temperature profile in the reservoir for different rock densities (360 days)

Chapter 4: Productivity Improvement of TMS Wells

4.1 Long-term Productivity Model

Well Productivity Model. Assuming that the oil in the pay zone is produced using multi-fractured horizontal wells, Li et al.'s (2019) well productivity model is employed in this study to predict well productivities. The model takes the following form:

$$Q_o = \frac{5.91\times10^{-3} n_f k_m h(\bar{p} - p_w)}{B_o \mu S_f \sqrt{c}\left[\frac{1}{1-e^{-\sqrt{c}x_f}} - \frac{1}{3x_f\sqrt{c})}\right)} \tag{4-1}$$

where c is expressed in US field units as

$$c = \frac{96k_m}{k_f w S_f} \tag{4-2}$$

where Q_o is oil production rate in stb/d, n_f is the number of fractures, k_m is matrix permeability in md, h is pay zone thickness in ft, $\bar{p}$ is the average formation pressure in psia, p_w is wellbore pressure in psia, B_o is oil formation volume factor, μ is fluid viscosity in cp, S_f is fracture spacing in ft, e is the exponential function, x_f is fracture half-length in ft, k_f is fracture permeability in md, and w is the average fracture width in inch. Equation (4-1) shows that well productivity is inversely proportional to oil viscosity. If the oil viscosity is reduced by 50% by the geothermal energy, it is expected that well productivity will be doubled.

Case Analysis. The proposed y-shaped well couple and the associated heat transfer models were used to investigate well productivity improvement in the TMS with the stimulation of

geothermal energy from a deeper depth. Table 4-1 lists the parameters used in the analysis. These data were found from recent literature of TMS studies (Berch, 2014; Hackley and Cardott, 2016; Lohr et al., 2016; Borrok et al., 2019; Yang and Guo, 2019).

Table 4-1: Data Set Used in Inter-wellbore Heat Transfer Calculations

Parameter	Value	Unit
Inner diameter of work pipe	0.1038	m
Thickness of work pipe	0.005207	m
Outer diameter of work pipe	0.1143	m
Clearance of wellbore annulus	0.02588	m
Thickness of cement sheath	0.02063	m
The cross-sectional area of the annulus in Sections I, II, and III	0.01139	m^2
The inner cross-sectional area of pipe in Sections I, II, and III	0.008471	m^2
Heat capacity of fluid in the annulus in Section I	4184	$J/(kg-℃)$
Heat capacity of work fluid	4100	$J/(kg-℃)$
Thermal conductivity of annulus fluid	0.598	$J/(kg-℃)$
Thermal conductivity of pipe	45	$W/(m-℃)$
Thermal conductivity of cement in Sections I and II	0.1	$W/(m-℃)$
Thermal conductivity of cement in Sections III and IV	0.54	$W/(m-℃)$
Fluid flow rate inside work pipe	0.004-0.01	m^3/s
Geothermal temperature at surface	20	℃
The temperature of work fluid at surface	40	℃
Work fluid density	1030	kg/m^3
Length of Section I	3600	m
Length of Section II	3400	m
Length of Section III	1000	m
Length of Section IV	1900	m
Cement sheath thickness in Section IV	0.04445	m
Outer diameter pipe in Section IV	0.1143	m
Inner cross-sectional area of casing in Section IV	0.008471	m^2
Producing wellbore diameter	0.15875	m
Reservoir depth	3600	m
Thermal gradient	0.022	$℃/m$

Figure 4-1 presents the model-calculated fluid temperature profiles for different flow rates of work fluids in the Section IV. It illustrates that the level of temperature increases with fluid flow rate, while the temperature drop along the section decreases with flow rate. At a flow rate of 0.01 m^3/s, the temperature of the work fluid is 171 °C at the inlet and 148 °C at the inlet of Section IV. According to Eq. (2-29), the heat flow rate from the wellbore to the reservoir is

$Q_{rw} = 991{,}190\ J/s$. This heat flow rate was employed for calculating the temperature raise in the oil reservoir using the analytical model expressed by Eq. (2-27). Model input data are presented in Table 4-2 (Berch, 2014; Hackley and Cardott, 2016; Borrok et al., 2019; Yang and Guo, 2019b). Figure 4-2 shows the temperature raise with time at difference radial distances from wellbore. It indicates that the heat transfer is a slow process due to the low thermal conductivity of reservoir rock and fluids. It will take 2 years for the reservoir temperature to increase from 99.3°C to 110°C in the radial distance of 10 m. Figure 4-3 presents temperature profiles in the reservoir at difference time of heat transfer. It demonstrates that the temperature in the vicinity of the wellbore increases quickly and stabilizes at high level.

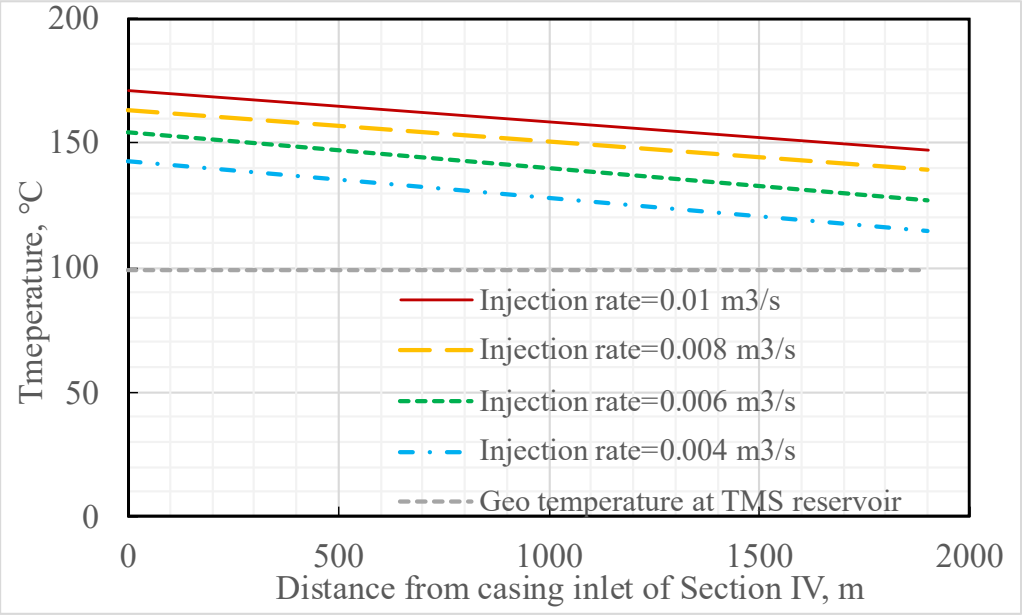

Figure 4-1: Temperature profiles of work fluid at different flow rates in Section IV

Table 4-2: Data Set Used in In-Reservoir Heat Transfer Calculations

Wellbore length	1900	m
Thermal conductivity of rock	5	W/m-°C
Density of rock	2650	kg/m^3
Heat capacity of pay zone	920	J/kg-C
Initial rock temperature	99.2	C

Work fluid density	1030	kg/m^3
Work fluid flow rate	0.01	m^3/s
Heat capacity of work fluid	4184	J/kg-C
Fluid temperature at inlet of wellbore	171	C
Fluid temperature at outlet of wellbore	148	C

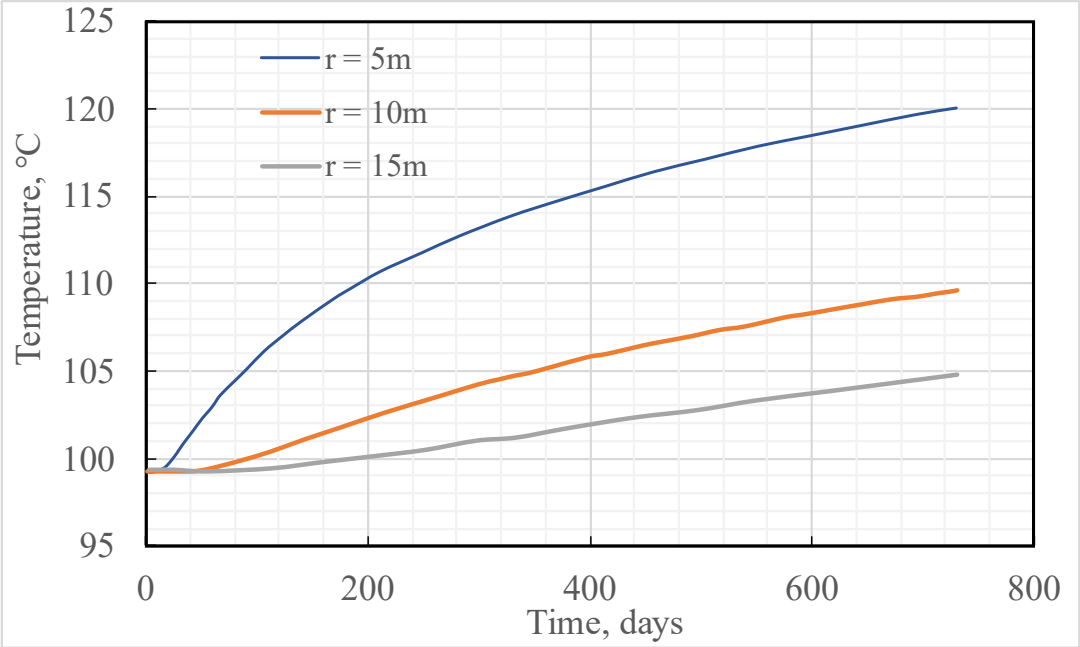

Figure 4-2: Temperature raise with time at difference radial distances from wellbore

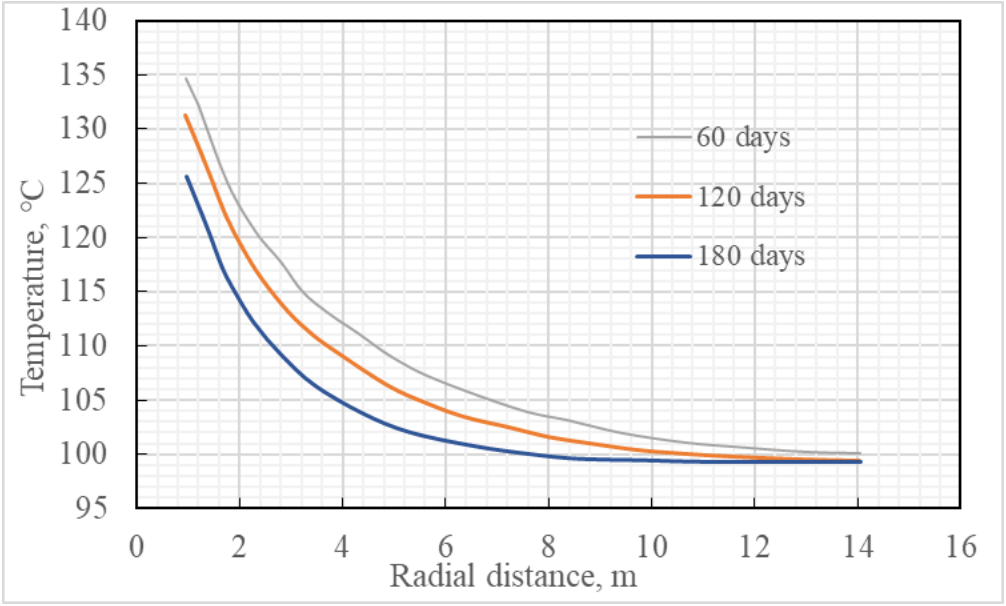

Figure 4-3: Temperature profiles in the reservoir at difference time of heat transfer

To quantify the effect of effect of temperature raise on the well productivity of TMS wells, it is essential to establish a relation between temperature and oil viscosity. Table 4-3 summarizes data utilized for calibrating Standing's correlation for oil viscosity (Yang and Guo, 2020). This correlation gives an oil viscosity of 0.39 cp which is 27% lower than the TMS oil viscosity 0.5 cp used by Yang and Guo (2020). Therefore, the Standing's correlation for oil viscosity was tuned by a factor of 1.27 for predicting oil viscosities of TMS oil at elevated temperatures. The calibrated correlation is presented in Figure 4-4 which indicates a sharp decline of oil viscosity with increased temperature. If the TMS reservoir temperature can be increased from 99.2°C to 171°C by the stimulation of geothermal energy, the oil viscosity is expected to drop from 0.5 cp to 0.22 cp.

Table 4-3: Data Set Used for Calibrating Standing's Correlation

Parameter	Value	Unit
Reservoir pressure	4980	$psia$
Reservoir temperature	210.56	°F
Oil bubble point pressure	4980	$psia$

Stock tank oil gravity	39	°API
Solution gas oil ratio	555	scf/stb
Gas specific gravity	0.7	$air = 1$

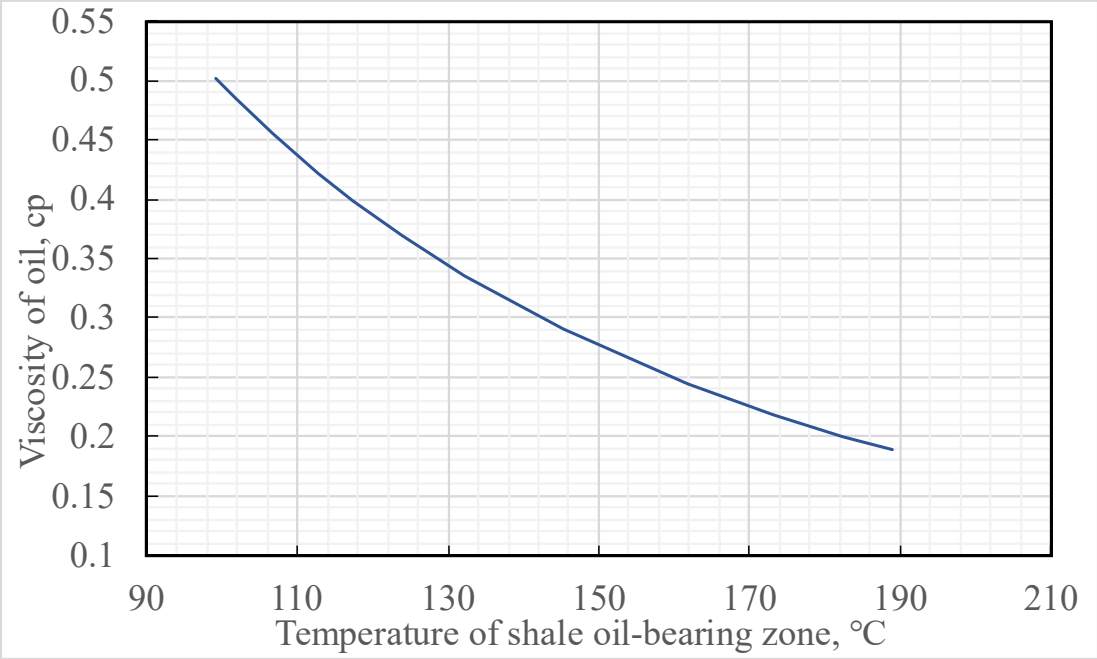

Figure 4-4: Effect of temperature on TMS oil viscosity based on calibrated Standing's correlation

Table 4-4 provides TMS reservoir property and well completion data that were used by previous investigators (John, 1997; Yang and Guo, 2020). Applying these data to Eq. (4-1) allowed for generating well production rate data shown in Figure 4-5. This figure demonstrates that oil production rate should increase sharply as oil viscosity drops due to the heating effect of geothermal energy brought from a deeper depth. If the oil viscosity is lowered from 0.5 cp to 0.22 cp, well productivity should be doubled from 140 stb/day to 320 stb/day.

Table 4-4: TMS Reservoir Property and Well Completion Data

Parameter	Value	Unit
Average horizontal wellbore length	**6375**	ft

Average fracture spacing	**62**	ft
Average fracture half-length	**234**	ft
Pay-zone thickness	**137**	ft
Reservoir effective permeability	**0.00016**	md
Formation pressure	**4980**	psi
Flowing bottom hole pressure	**3600**	psi
Oil formation factor	**1.3**	rb/stb
Fracture permeability	**30000**	md
Number of hydraulic fractures per well	**104**	
Fracture width	**0.012**	$inch$
Gas specific gravity	**0.7**	$air = 1$

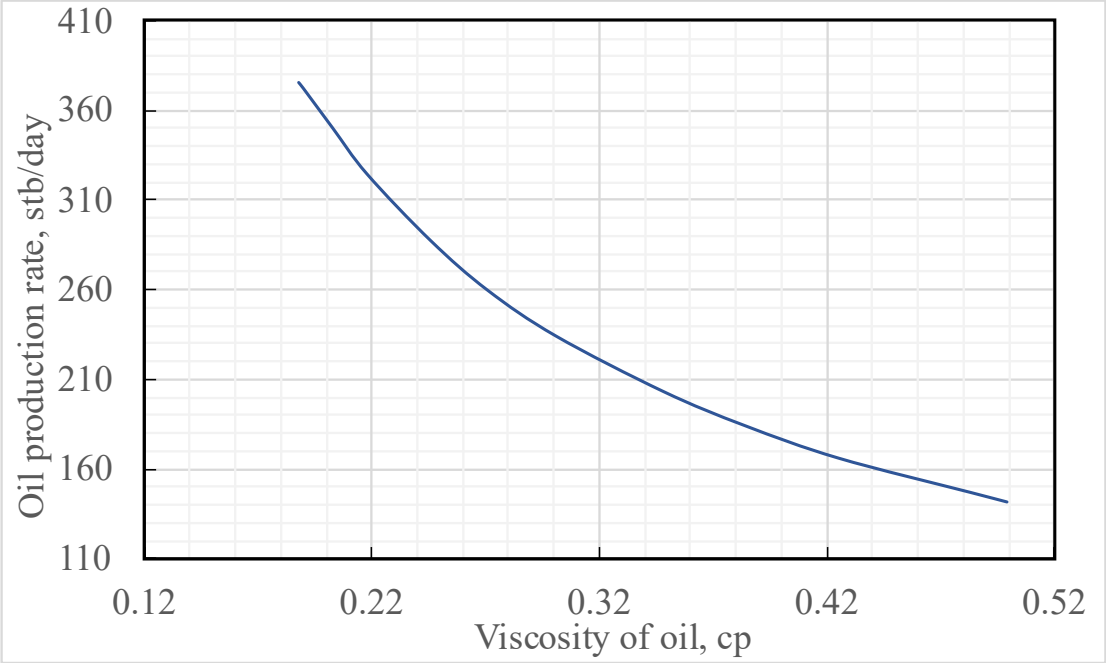

Figure 4-5: Model-predicted oil production rate at different oil viscosities

4.2 Sensitivity Analysis

Sensitivity analysis is the study of how the production rate in the output of the mathematical model (Eq.4-1) can be affected by its input parameters. This is a simulation method to predict the outcome of a decision given a certain range of variables. Through this analysis, we can

understand which parameters affected the production rate more than others, and then optimize the correspondingly parameters if they are adjustable.

4.2.1 Effect of Fractures

For the development of shale reservoirs, Hydraulic fracturing is a necessary engineering method. The man-made fractures can determine the permeability near the wellbore and the well production rate. Therefore, in this section, we do the sensitivity analysis on production rate by checking the fracture related parameters. There are three key indexes to affect the production rate in this research including the fracture width, the fracture half-length, fracture permeability, and fracture spacing.

Fracture width. Fracture width, also known as average fracture width, is one of the most important parameters for describing fracture status and measuring the effect of hydraulic fracturing (Ran et al., 2014). It represents the difficulty level of the formation fluid flowing to wellbore through the horizontal section. Therefore, production rate is a function of average fracture width. Figure 4-6 indicates the relationship of production rate and oil viscosity in near-wellbore formation at different fracture widths. The vertical axis shows the production rate, while horizontal axis represents the viscosity of oil in TMS formation. The smooth curves represent the trend of production rate change along with the viscosity of oil. Overall, the production rate is negatively related to the viscosity of oil. The production rate is decreasing with a decreasing slope along with the increasing of oil viscosity. Considering the viscosity of oil from 0.2 cp to 0.5 cp, the production rate with the average fracture width of 0.012 inch in rock, decreases from 352 stb/day to 140 stb/day, so the difference is 212 stb/day, while with the average fracture width of 0.002 inch, the production rate decreases from 292 stb/day to 117 stb/day, so the difference is 175 stb/day. Comparing with the two

fracture widths of the rock, it shows that the wider fracture, the higher production rate in the wellbore. And on the other hand, the wider fracture width leads to bigger production rate changes in the wellbore, when the viscosity of oil changes. The increments of fracture width and production rate are not linear, since when the fracture width increases from 0.002 inch to 0.012 inch causes higher increment of production rate than it increases from 0.012 inch to 0.022 inch. Considering the optimization of energy transfer process, the bigger fracture width is beneficial to oil transfer.

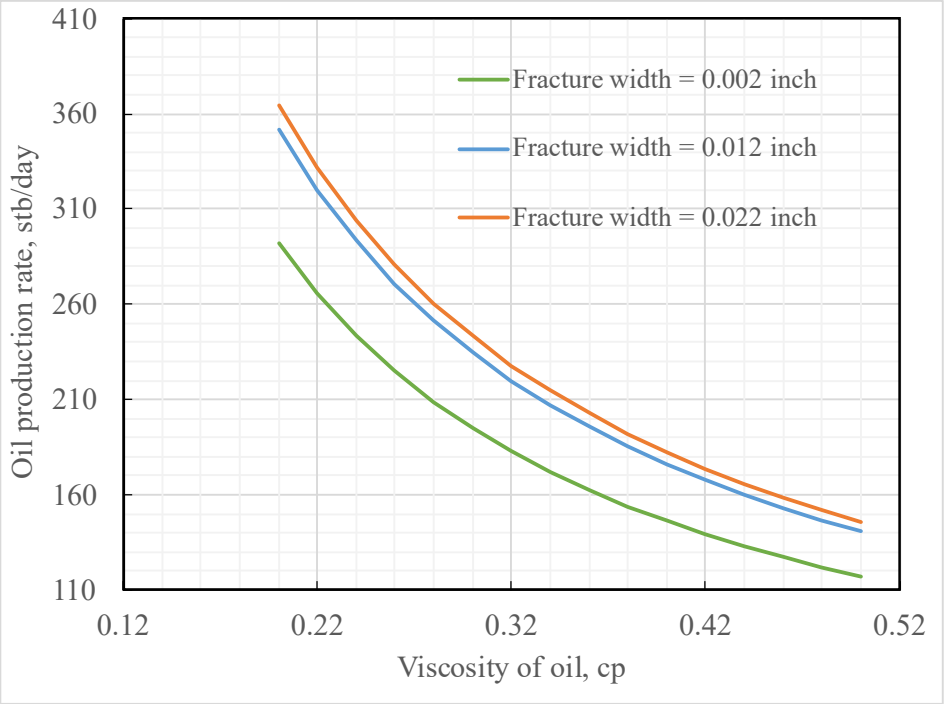

Figure 4-6: Effect of fracture width

Fracture half-length. Fracture half-length is the length of one wind of a fracture from the wellbore to the tip (Yu and Sepehmoori, 2018; Barree et al., 2005). It is also one of the most important parameters for describing fracture status and measuring the effect of hydraulic fracturing. It represents the degree of difficulty of the formation fluid flowing to wellbore

through the horizontal section. Therefore, production rate is a function of fracture half-length. Figure 4-7 indicates the relationship of production rate and oil viscosity in near-wellbore formation at different fracture half-lengths. The smooth curves represent the trend of production rate change along with the viscosity of oil. Overall, the production rate is negatively related to the viscosity of oil. The production rate is decreasing with a decreasing slope along with the increasing of oil viscosity. Considering the viscosity of oil from 0.2 cp to 0.5 cp, the production rate with the fracture half-length of 264 ft in rock, decreases from 390 stb/day to 156 stb/day, so the difference is 234 stb/day, while with the fracture half-length of 204 ft, the production rate decreases from 312 stb/day to 125 stb/day, so the difference is 187 stb/day. Comparing with the two fracture half-lengths of the rock, it shows that the longer fracture half-length, the higher production rate in the wellbore. And on the other hand, the longer fracture half-length leads to bigger production rate changes in the wellbore, when the viscosity of oil changes. The increments of fracture half-length and production rate are about linear, since when the fracture half-length increases 30 ft, the production rate increases about 30 stb/day. Considering the optimization of energy transfer process, the longer fracture half-length is beneficial to oil transfer.

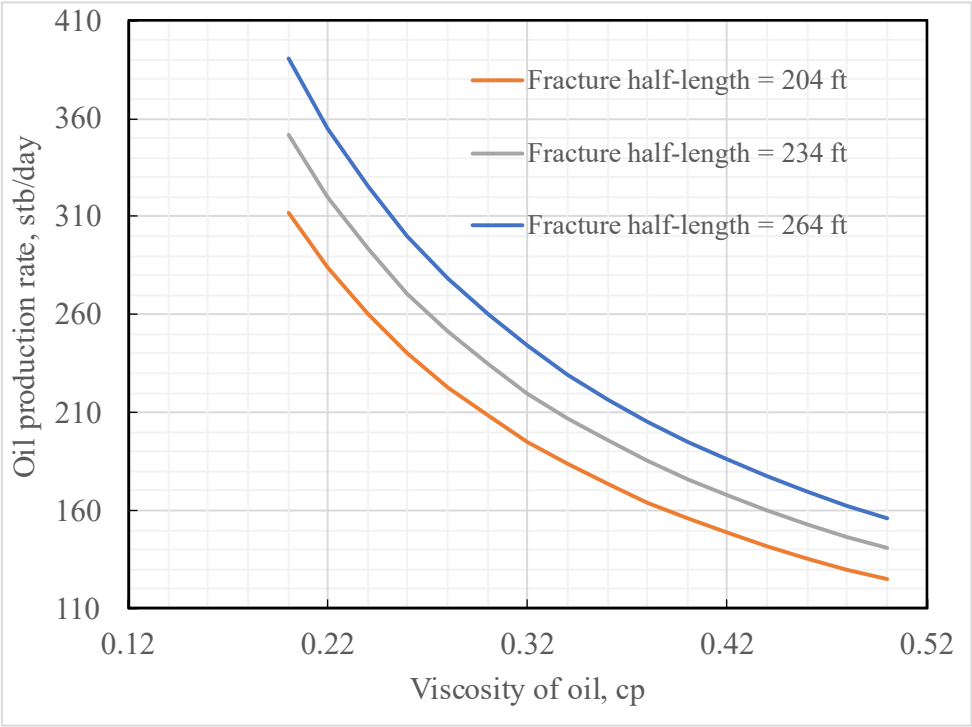

Figure 4-7: Effect of fracture half-length

Fracture permeability. Fracture permeability, also known as fracture conductivity, is a measure of how easily fluids flow through a fracture (Carey et al.,2015; Walsh,1981). It can be used to measure the effect of hydraulic fracturing. Figure 4-8 indicates the relationship of production rate and oil viscosity in near-wellbore formation at different fracture permeabilities. The smooth curves represent the trend of production rate change along with the viscosity of oil. Overall, the production rate is negatively related to the viscosity of oil. The production rate is decreasing with a decreasing slope along with the increasing of oil viscosity. Considering the viscosity of oil from 0.2 cp to 0.5 cp, the production rate with the fracture permeability of 20,000 md in rock, decreases from 342 stb/day to 137 stb/day, so the difference is 205 stb/day, while with the fracture permeability of 40,000 md, the production rate decreases from 358 stb/day to 143 stb/day, so the difference is 215 stb/day. Comparing

with the two fracture permeabilities of the rock, it shows that when fracture permeability increases, the production rate slightly increases in the wellbore. And on the other hand, the production rate is not sensitive to the fracture permeability when the viscosity of oil changes. The increments of fracture permeability and production rate are not linear, since when the fracture permeability increases from 20,000 md to 30,000 md causes higher increment of production rate than it increases from 30,000 md to 40,000 md. Considering the optimization of energy transfer process and reducing the engineering costs, the higher fracture permeability means a slightly higher production rate but a higher engineering cost. Therefore, a relatively lower fracture permeability (20, 000 md) is the best option from the angle of economy.

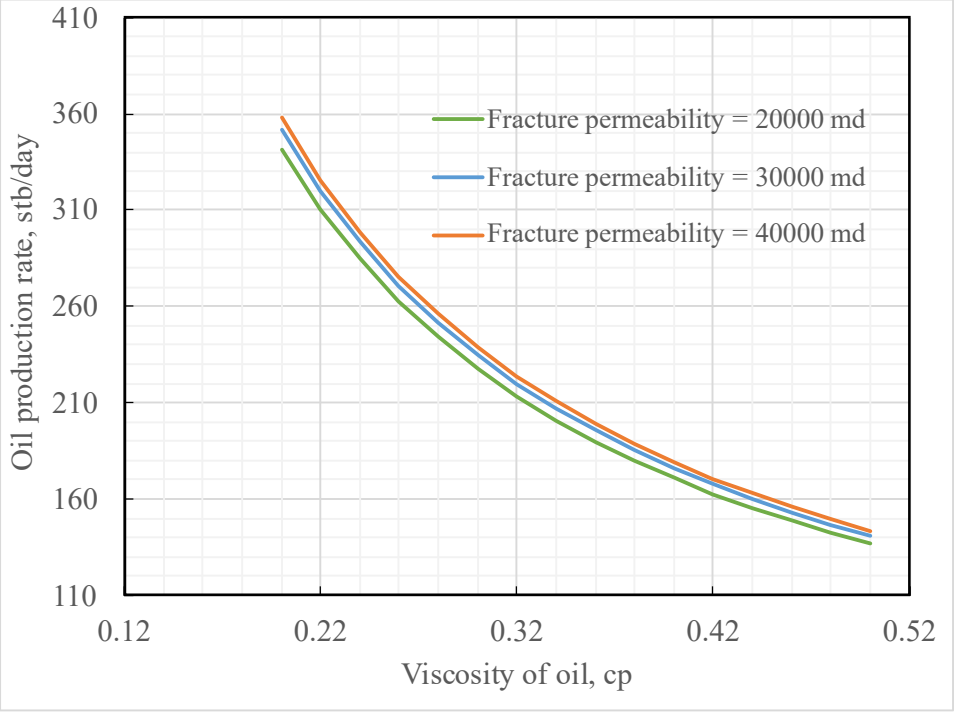

Figure 4-8: Effect of fracture permeability

Fracture spacing. Fracture spacing, also known as fracture intensity, means the distance between fractures for a unit length of oil formation (Dershowitz and Herda,1992; Narr,1996). It can be determined by perforation density in hydraulic fracturing design. Fracture spacing is not a direct measure the effect of hydraulic fracturing, but it is an important index to affect production rate in shale formations. Figure 4-9 indicates the relationship of production rate and oil viscosity in near-wellbore formation at different fracture spacings. The smooth curves represent the trend of production rate change along with the viscosity of oil. Overall, the production rate is negatively related to the viscosity of oil. The production rate is decreasing with a decreasing slope along with the increasing of oil viscosity. Considering the viscosity of oil from 0.2 cp to 0.5 cp, the production rate with the fracture spacing of 52 ft in rock, decreases from 414 stb/day to 166 stb/day, so the difference is 248 stb/day, while with the fracture spacing of 72 ft, the production rate decreases from 306 stb/day to 122 stb/day, so the difference is 184 stb/day. Comparing with the two fracture spacings of the rock, it shows that when fracture spacing decreases, the production rate increases in the wellbore. And on the other hand, the smaller fracture spacing leads to bigger production rate changes in the wellbore, when the viscosity of oil changes. The increments of fracture spacing, and production rate are not linear, since when the fracture spacing increases from 52 ft to 62 ft causes higher increment of production rate than it increases from 62 ft to 72 ft. Considering the optimization of energy transfer process, the smaller fracture spacing is beneficial to oil transfer.

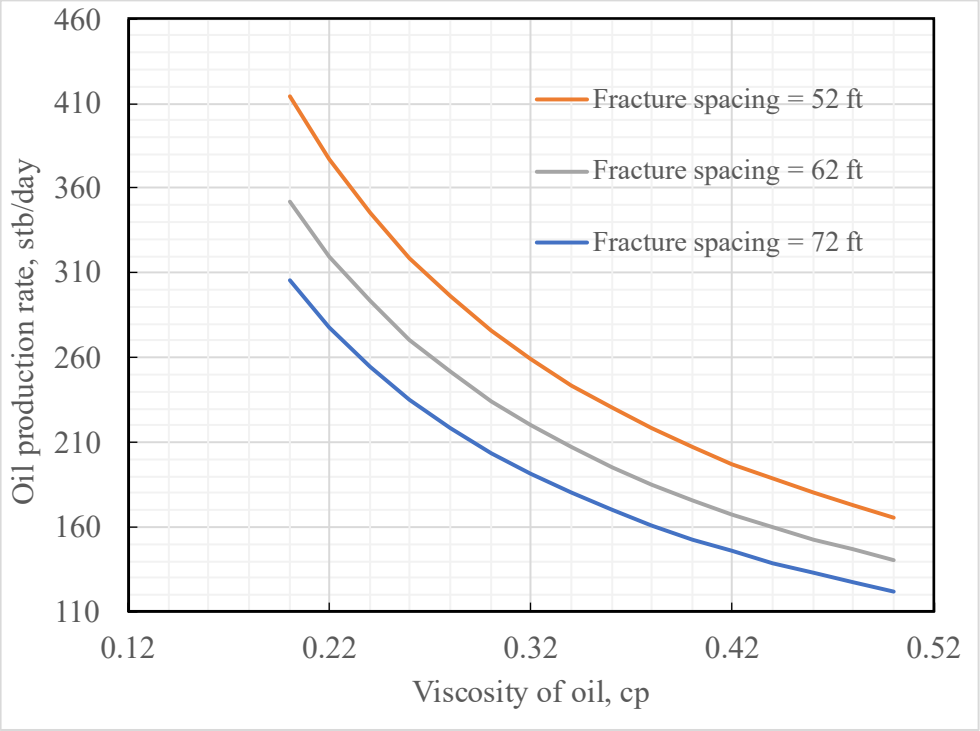

Figure 4-9: Effect of fracture spacing

Number of Fractures. Number of Fractures means the total number of fractures in the perforation area. It relates to the concept of fracture spacing, but it is different from fracture spacing. Number of fractures emphasizes the number, while fracture spacing underlines the density of fractures. Number of fractures can be determined by perforation design in well completion design. Number of fractures is not a direct measure the effect of hydraulic fracturing, but it is an important index to affect production rate in shale formations. Figure 4-10 indicates the relationship of production rate and oil viscosity in near-wellbore formation at different numbers of fractures. The smooth curves represent the trend of production rate change along with the viscosity of oil. Overall, the production rate is negatively related to the viscosity of oil. The production rate is decreasing with a decreasing slope along with the increasing of oil viscosity. Considering the viscosity of oil from 0.2 cp to 0.5 cp, the

production rate with the fracture number of 84 in rock, decreases from 284 stb/day to 114 stb/day, so the difference is 170 stb/day, while with the fracture number of 124, the production rate decreases from 420 stb/day to 168 stb/day, so the difference is 252 stb/day. Comparing with the two fracture numbers of the formation, it shows that when number of fractures increases, the production rate increases in the wellbore. And on the other hand, the larger number of fractures leads to higher production rate changes in the wellbore, when the viscosity of oil changes. The increments of number of fractures and production rate are about linear, since when the number of fractures increases from 84 to 104 causes the same increment of production rate as it increases from 104 to 124. Considering the optimization of energy transfer process, the larger number of fractures is beneficial to oil transfer.

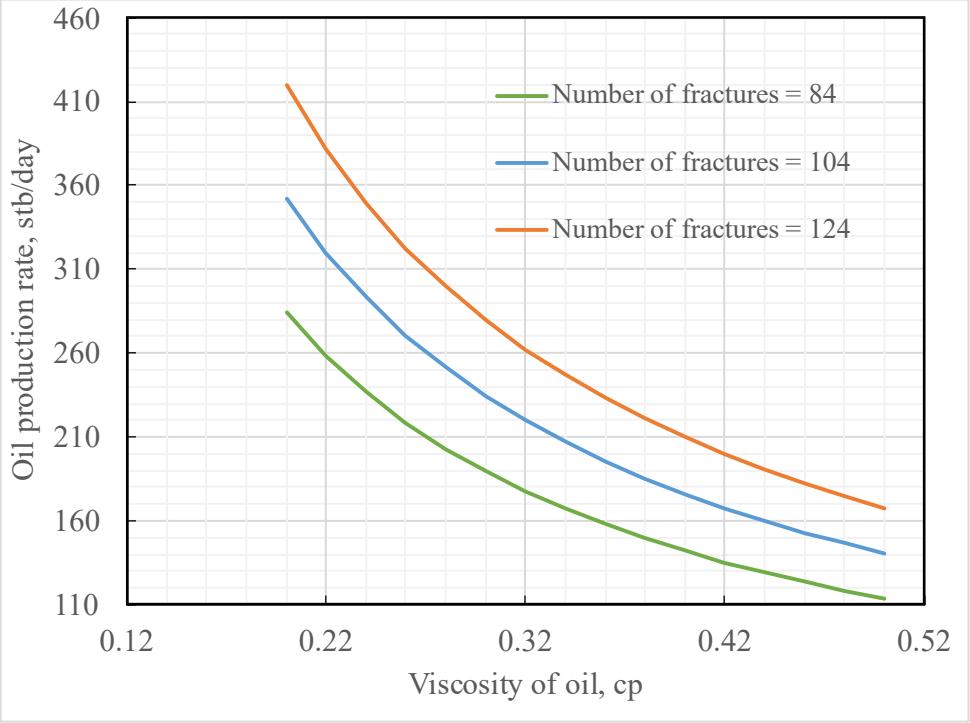

Figure 4-10: Effect of number of fractures

4.2.2 Effect of Formation Property

Matrix permeability. Matrix permeability of shale reservoir rocks is a measure of the ability of a porous shale rock to allow oil to pass through it (Luffel et al.,1993; Castellon and Sieving, 2006; Bodin et al., 2003). Matrix permeability relates to effective porosity. It is determined by the effective porosity, lithology, and mineral composition. It is an unchangeable parameter, However, doing research on this parameter helps us understand the shale formation and optimize hydraulic fracturing. In general, the matrix permeability of shale is low, which is harmful to the oil transfer in shale matrix. The objective of hydraulic fracturing is increasing the average permeability of the formation by creating cracks. Matrix permeability can be measured by Darcy's experiments. It characterizes the flow status of oil in the original formation before hydraulic fracturing. Figure 4-11 indicates the relationship of production rate and oil viscosity in near-wellbore formation at different numbers of fractures. The smooth curves represent the trend of production rate change along with the viscosity of oil. Overall, the production rate is negatively related to the viscosity of oil. The production rate is decreasing with a decreasing slope along with the increasing of oil viscosity. Considering the viscosity of oil from 0.2 cp to 0.5 cp, the production rate with the matrix permeability of 0.00014 md in rock, decreases from 311 stb/day to 124 stb/day, so the difference is 187 stb/day, while with the matrix permeability of 0.00018 md, the production rate decreases from 393 stb/day to 157 stb/day, so the difference is 236 stb/day. Comparing with the two matrix permeabilities of the formation, it shows that when matrix permeability increases, the production rate increases in the wellbore. And on the other hand, the larger matrix permeability leads to higher production rate changes in the wellbore, when the viscosity of oil changes. The increments of matrix permeability and production rate are about

linear, since when the matrix permeability increases from 0.00014 md to 0.00016 md causes the same increment of production rate as it increases from 0.00016 md to 0.00018 md. Considering the optimization of energy transfer process, the larger matrix permeability is beneficial to oil transfer.

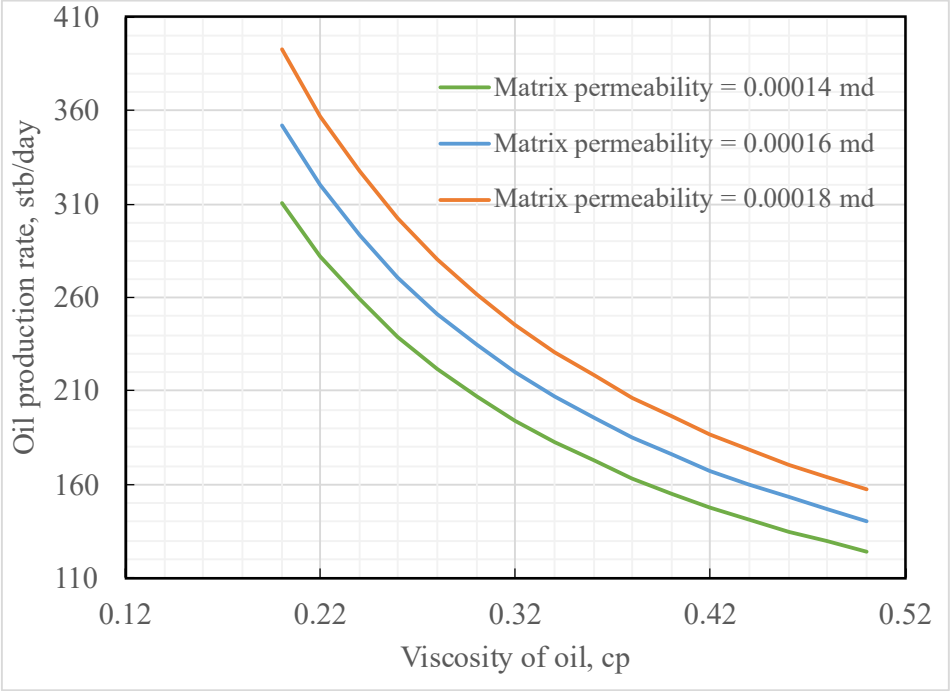

Figure 4-3: Effect of matrix permeability

Pay zone thickness. Pay zone thickness of the shale reservoir is the thickness of a shale reservoir or part of a shale reservoir that offers extracted hydrocarbons to a production wellbore (Tajali and Arian, 2016). It is an unchangeable parameter, However, doing research on this parameter helps us understand the shale formation and optimize hydraulic fracturing. Pay zone thickness cannot be measured directly, but it can be obtained by the indirect method like 3D seismic surveying and logging. Figure 4-12 indicates the relationship of production rate and oil viscosity in near-wellbore formation at different numbers of fractures. The

smooth curves represent the trend of production rate change along with the viscosity of oil. Overall, the production rate is negatively related to the viscosity of oil. The production rate is decreasing with a decreasing slope along with the increasing of oil viscosity. Considering the viscosity of oil from 0.2 cp to 0.5 cp, the production rate with the pay zone thickness of 117 ft in rock, decreases from 301 stb/day to 120 stb/day, so the difference is 181 stb/day, while with the pay zone thickness of 157 ft, the production rate decreases from 403 stb/day to 161 stb/day, so the difference is 242 stb/day. Comparing with the two pay zone thicknesses of the formation, it shows that the higher pay zone thickness, the higher production rate in the wellbore. And on the other hand, the higher pay zone thickness leads to higher production rate changes in the wellbore, when the viscosity of oil changes. The increments of pay zone thickness and production rate are about linear, since when the pay zone thickness increases from 117 ft to 137 ft causes the same increment of production rate as it increases from 137 ft to 157 ft. Considering the optimization of energy transfer process, the larger pay zone thickness has more producing potentials.

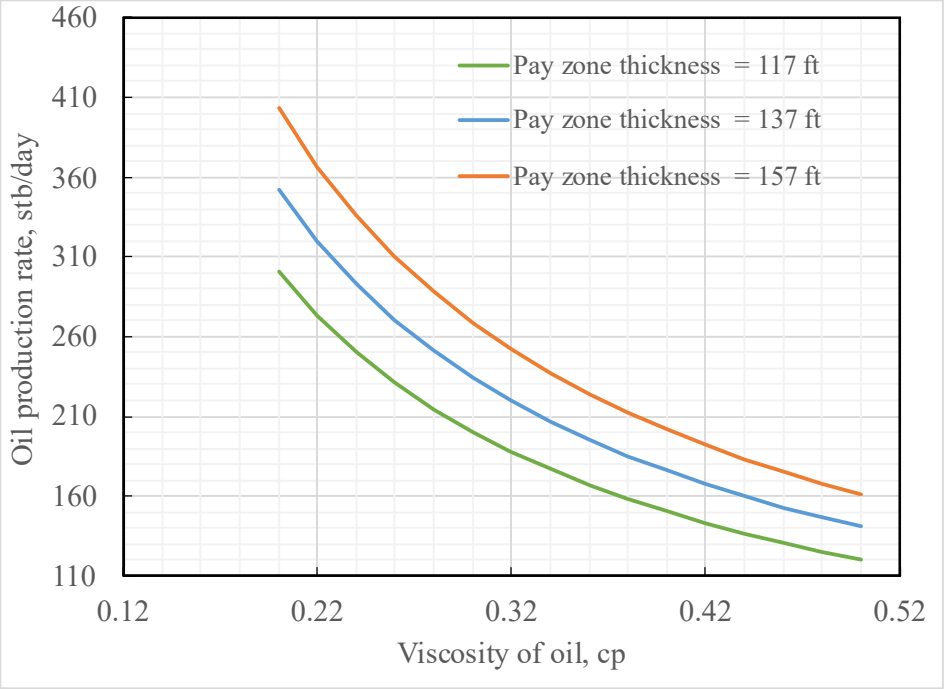

Figure 4-4: Effect of pay zone thickness

Formation pressure. Formation pressure is the pressure acting on the fluids including water, oil, and gas in the pore space of the formation (Ahmed et al.,2019; Thomson et al.,2021; Abdelaal et al.,2022). There are two types of formation pressures. One is normal formation pressure, while the other one is abnormal formation pressure (eg. high-temperature and high-pressure formation). Normal formation pressure is calculated by the formation pressure gradient times the formation depth. Shale oil and gas are often stored in the abnormal pressure formation. Doing research on formation pressure helps us understand the shale formation and optimize hydraulic fracturing. Figure 4-13 indicates the relationship of production rate and oil viscosity in near-wellbore formation at different numbers of fractures. The smooth curves represent the trend of production rate change along with the viscosity of oil. Overall, the production rate is negatively related to the viscosity of oil. The production rate is decreasing with a decreasing slope along with the increasing of oil viscosity.

Considering the viscosity of oil from 0.2 cp to 0.5 cp, the production rate with the formation pressure of 4780 psi, decreases from 301 stb/day to 120 stb/day, so the difference is 181 stb/day, while with the formation pressure of 5180 psi, the production rate decreases from 403 stb/day to 161 stb/day, so the difference is 242 stb/day. Comparing with the two formation pressures, it shows that the higher formation pressure, the higher production rate in the wellbore. And on the other hand, the higher formation pressure leads to higher production rate changes in the wellbore, when the viscosity of oil changes. The increments of formation pressure and production rate are about linear, since when the formation pressure increases from 4780 psi to 4980 psi causes the same increment of production rate as it increases from 4980 psi to 5180 psi. Considering the optimization of energy transfer process, the larger formation pressure is beneficial to oil transfer.

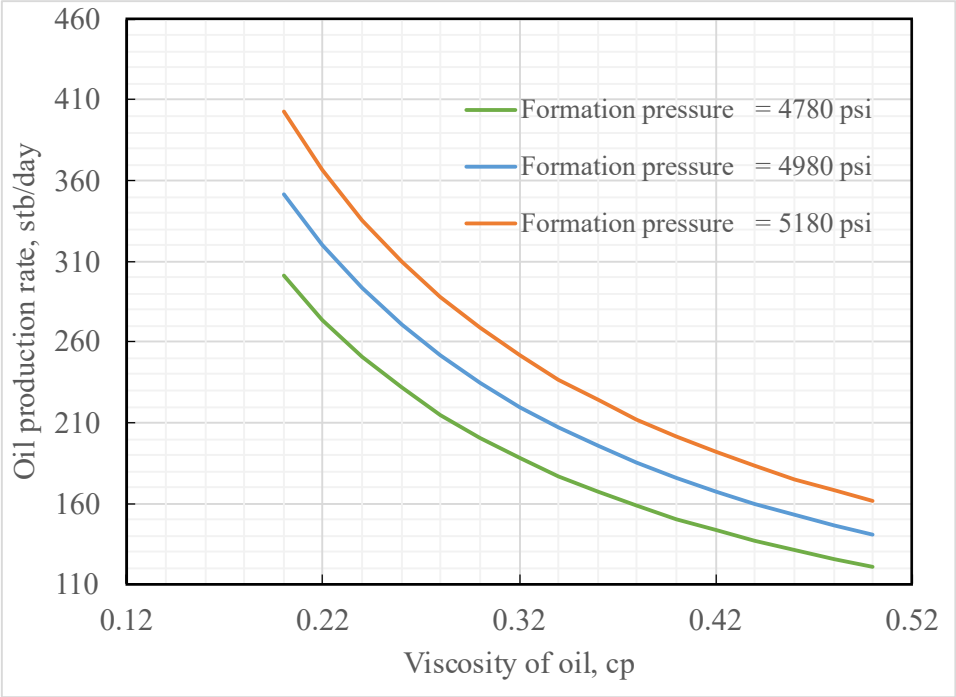

Figure 4-5: Effect of formation pressure

Oil formation volume factor. Oil formation volume factor is defined as oil and dissolved gas volume at reservoir temperature and pressure divided by the volume of the same sample at the standard conditions (Mahdiani and Norouzi, 2018; Ayoub et al.,2022; Wood and Choubineh, 2019). Oil formation volume factor is impacted by temperature, crudie oil gravity, and gas gravity. It is an unchangeable parameter, However, doing research on this parameter helps us understand the shale formation and optimize hydraulic fracturing. It can be obtained by experiments. Figure 4-14 indicates the relationship of production rate and oil viscosity in near-wellbore formation at different numbers of fractures. The smooth curves represent the trend of production rate change along with the viscosity of oil. Overall, the production rate is negatively related to the viscosity of oil. The production rate is decreasing with a decreasing slope along with the increasing of oil viscosity. Considering the viscosity of oil from 0.2 cp to 0.5 cp, the production rate with the oil formation volume factor of 1.2, decreases from 381 stb/day to 153 stb/day, so the difference is 228 stb/day, while with the oil formation volume factor of 1.4, the production rate decreases from 327 stb/day to 131 stb/day, so the difference is 196 stb/day. Comparing with the two oil formation volume factors of the formation, it shows that when oil formation volume factor decreases, the production rate increases in the wellbore. And on the other hand, the smaller oil formation volume factor leads to higher production rate changes in the wellbore, when the viscosity of oil changes. The increments of oil formation volume factor and production rate are not linear, since when the oil formation volume factor increases from 1.2 to 1.3 causes the bigger increment of production rate than it increases from 1.3 to 1.4. Considering the optimization

of energy transfer process, the smaller oil formation volume factor is beneficial to oil transfer.

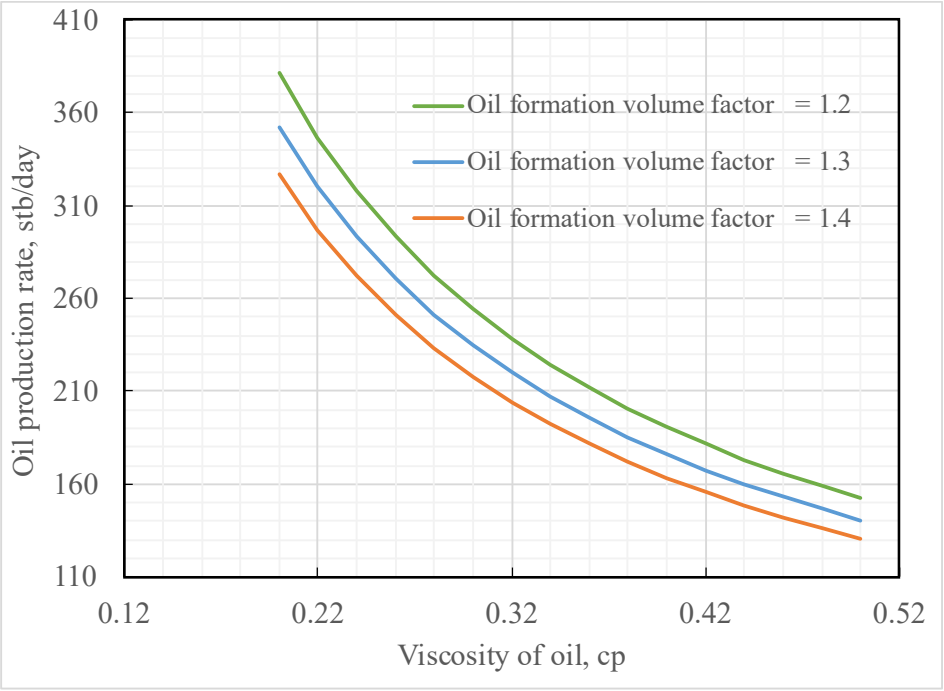

Figure 4-6: Effect of oil formation volume factor

4.2.3 Effect of Wellbore Pressure

Wellbore pressure, also known as bottomhole pressure, is the pressure at the bottom of a well. It is an adjustable parameter. In production wells, wellbore pressure can be controlled by changing the oil flow rate from the surface. Doing research on this parameter helps us understand the shale formation and optimize production process. Figure 4-15 indicates the relationship of production rate and oil viscosity in near-wellbore formation at different numbers of fractures. The smooth curves represent the trend of production rate change along with the viscosity of oil. Overall, the production rate is negatively related to the viscosity of

oil. The production rate is decreasing with a decreasing slope along with the increasing of oil viscosity. Considering the viscosity of oil from 0.2 cp to 0.5 cp, the production rate with the wellbore pressure of 3200 psi, decreases from 454 stb/day to 182 stb/day, so the difference is 272 stb/day, while with the wellbore pressure of 4000 psi, the production rate decreases from 250 stb/day to 100 stb/day, so the difference is 150 stb/day. Comparing with the two wellbore pressures, it shows that the lower wellbore pressure, the higher production rate in the wellbore. And on the other hand, the lower wellbore pressure leads to higher production rate changes in the wellbore, when the viscosity of oil changes. The increments of wellbore pressure and production rate are about linear, since when the wellbore pressure increases from 3200 psi to 3600 psi causes the same increment of production rate as it increases from 3600 psi to 4000 psi. Considering the optimization of energy transfer process, the lower wellbore pressure is beneficial to oil transfer.

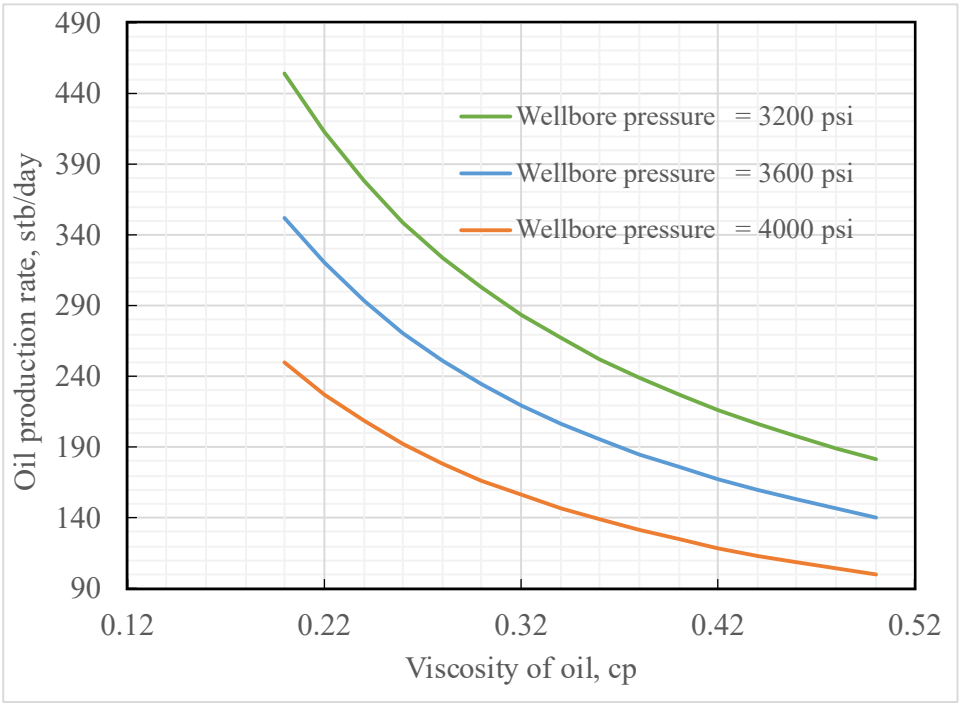

Figure 4-7: Effect of wellbore pressure

Chapter 5: Conclusions

In this research, we applied analytical and numerical methods to gain the knowledge of using geothermal energy to increase the temperature of TMS, thus decrease the viscosity of oil, and eventually increase the shale oil well productivity. We propose to use y-shaped well couples to transfer heat energy from a geothermal zone to the oil reservoir. Sensitivity analyses were performed to investigate the factors/parameters affecting heat transfer and well productivity improvement. The following conclusions are drawn.

1. Using y-shaped well couples to transfer the geothermal energy in a deeper depth to the TMS can reduce TMS oil viscosity from 0.5 cp to 0.22 cp. This reduction in oil viscosity is translated to an increase of initial oil production rate from 140 stb/day to 320 stb/day.

2. In the y-shaped well couples the flow rate of work fluid is a key factor affecting the heat transfer from the geothermal zones to the heat dissipator wellbores placed in the oil reservoir. While the high flow rate brings more volume of hot fluid from the geothermal zone to the dissipator wellbore, the temperature drop along the wellbore decreases slightly, reducing the time of heat transfer. Long oil production wellbores should be drilled to ensure adequate retention time for heat transfer.

3. Increasing the depth of the geothermal zone does not effectively increase the fluid temperature delivered to the oil pay zone due to the heat loss in the heat transfer wellbore

(Section II). Insulation of the heat transfer wellbore can significantly elevate the fluid temperature delivered to the oil pay zone.

4. The heat transfer from the heat dissipator wellbore to the oil reservoir is a slow process due to the low-thermal conductivity of reservoir rock and fluids. It should take about 2 years for the reservoir temperature to increase from 99.2^{o}C to 110^{o}C everywhere within a radial distance of 10 m. However, the temperature in the vicinity of the heat dissipator wellbore increases quickly and stabilizes at high level, suggesting no need to wait for heat transfer prior to oil production from the production wellbore if the production wellbore is placed in a few meters to the heat dissipator wellbore.

5. For a given oil reservoir, fracture properties play important roles on oil production rate. Higher average fracture width, longer fracture half length, higher fracture permeability, less fracture spacing, larger number of fractures are all favorable for improving oil production rate.

Chapter 6: Commercialization

6.1 Market for Commercialization

To meet the need of energy in the coming couple of years and solve oil shortage, increasing the supply of the United States oil and natural gas resources is a sustainable development method. TMS, on top of emerging shale plays, is an prospective shale play with estimated 7 billion bbls of oil. Currently, the production rate of the TMS is nearly 3000 bbl of oil per day. Therefore, it still has a huge potential for shale oil production in the future (John et al., 1997).

Horizontal drilling and hydraulic fracturing as the key technological innovation achievements in shale oil and gas extraction have made tremendous success. According to statistics, between the year 2007 and the year 2013, the production of the shale gas led to an increase in social welfare for the consumers and producers of 48 billion dollars per year, but more data are needed on the extent and valuation of the environmental impacts of shale gas production (Hausman and Kellogg, 2015).

The Tuscaloosa Marine Shale region of Louisiana and Mississippi is an economic undeveloped area. The population of this region has declined in the last five years and is expected to have anemic growth lagging behind average growth in the United States. According to data statistics, 60% of the population in the rural southern regions merely have a high school diploma or even less. The unemployed population is over 17,000. The region has lost over 6,000 job opportunities in the last five years. By far the largest and second largest employer in the region are government and retail, respectively. The largest exporting

industries are logging, poultry, and crop production. Some economic developers believe that direct local job creation from shale gas and oil extraction will be modest, as most jobs come from processing and manufacturing to serve the industry (Miller and Bolton, 2016).

However, the oil companies and service companies need to hire a large number of works for well drilling and oil-field development. The researchers are needed to develop and apply innovation techniques to optimize the shale oil production. More local schools and colleges will be built for training workers and highly educated researchers. The intellectual property of developing the TMS will also bring wealth to Louisiana and Mississippi. These regions can have an economic boost by developing shale oil (Qun et al., 2022).

6.2 Completed Work in Commercialization

Data and knowledge dissemination is an important stage of commercialization of research result. Three papers have been published in journals for dissemination of knowledge to the oil industry and academia. These papers are:

Zhang, He, et al. "Analyzing the Validity of Brazilian Testing Using Digital Image Correlation and Numerical Simulation Techniques." *Energies* 13.6 (2020): 1441.

Guo, B. and Zhang, H. "|Mathematical Modeling of Heat Transfer from Geothermal Zones to Natural Gas Hydrate Reservoirs." Petroleum & Petrochemical Engineering Journal (February 24, 2022), Vol. 6, Issue 1. DOI: 10.23880/ppej-16000296.

Guo, B. and Zhang, H. “Mathematical Modeling of the Dynamic Temperature Profile in Geothermal-Energy-Heated Natural Gas Hydrate Reservoirs.” *Sustainability* (2022), 14, 2767. https://doi.org/10.3390/su14052767.

In addition, computer software development for the end-users is also an important stage of commercialization of research result. The computer program package developed in this work has been illustrated to private sectors in the oil industry, including the Pegasus Vertex, Inc.

Reference

Abdelaal, A., Elkatatny, S. and Abdulraheem, A., 2022. Real-time prediction of formation pressure gradient while drilling. Scientific Reports, 12(1), pp.1-14.

Ahmed, A., Elkatatny, S., Ali, A. and Abdulraheem, A., 2019. Comparative analysis of artificial intelligence techniques for formation pressure prediction while drilling. Arabian Journal of Geosciences, 12(18), pp.1-13.

Allen Jr., J.E., Meylan, M.A. and Heitmuller, F.T. 2014. Determining Hydrocarbon Distribution Using Resistivity, Tuscaloosa Marine Shale, Southwestern Mississippi. Gulf Coast Association of Geological Societies Transactions 64: 41–57.

Ambrose, W.A., Loucks, R.G., and Dutton, S.P. 2015. Sequence-Stratigraphic and Depositional Controls on Reservoir Quality in Lowstand Incised-Valley Fill and Highstand Shallow-Marine Systems in the Upper Cretaceous (Cenomanian) Tuscaloosa Formation, Louisiana, USA. *GCAGS Trans* **4**: 43–63.

Ayoub, M.A., Elhadi, A., Fatherlhman, D., Saleh, M.O., Alakbari, F.S. and Mohyaldinn, M.E., 2022. A new correlation for accurate prediction of oil formation volume factor at the bubble point pressure using Group Method of Data Handling approach. *Journal of Petroleum Science and Engineering*, *208*, p.109410.

Babar, H., Sajid, M.U. and Ali, H.M., 2019. Viscosity of hybrid nanofluids: a critical review. *Thermal Science*, *23*(3 Part B), pp.1713-1754.

Barree, R.D., Cox, S.A., Gilbert, J.V. and Dobson, M., 2005. Closing the gap: Fracture half length from design, buildup, and production analysis. SPE Production & Facilities, 20(04), pp.274-285.

Barrell, K.A. 2013. The Tuscaloosa Marine Shale an Emerging Shale Play. *Houston Geological Society Bulletin* **55**(6): 43–45.

Beggs, H.D. and Robinson, J.R., 1975. Estimating the viscosity of crude oil systems. *Journal of Petroleum technology*, 27(09), pp.1140-1141.

Berch, H. and Nunn, J. 2014. Predicting Potential Unconventional Production in the Tuscaloosa Marine Shale Play Using Thermal Modeling and Log Overlay Analysis. *GCAGS Trans* **64**: 69–78.

Bodin, J., Delay, F. and De Marsily, G., 2003. Solute transport in a single fracture with negligible matrix permeability: 1. fundamental mechanisms. Hydrogeology journal, 11(4), pp.418-433.

Borrok, D. M., Yang, W., Wei, M. et al. 2019. Heterogeneity of the Mineralogy and Organic Content of the Tuscaloosa Marine Shale. *Mar Petrol Geol* **109**: 717–731. https://doi.org/10.1016/j.marpetgeo.2019.06.056.

Carey, J.W., Lei, Z., Rougier, E., Mori, H. and Viswanathan, H., 2015. Fracture-permeability behavior of shale. Journal of unconventional oil and gas resources, 11, pp.27-43.

Castellón, T.D. and Sieving, K.E., 2006. An experimental test of matrix permeability and corridor use by an endemic understory bird. *Conservation biology*, *20*(1), pp.135-145.

De Ghetto, G., Paone, F. and Villa, M., 1995, June. Pressure-volume-temperature correlations for heavy and extra heavy oils. In *SPE International Heavy Oil Symposium*. OnePetro.

Dershowitz, W.S. and Herda, H.H., 1992, June. Interpretation of fracture spacing and intensity. In *The 33rd US Symposium on Rock Mechanics (USRMS)*. OnePetro.

Durham, L.S. 2013. Geologists Excited About TMS Potential. *AAPG Explorer* **34**(7): 16–18.

Durham, L.S. 2014. Little Known TMS Play Sees Drilling Surge. *AAPG Explorer* **35**(8): 12–16.

Durham, L.S. 2015. Oil Price Slams Beleaguered TMS play. *AAPG Explorer* **36**: 46.

Fu, C., Guo, B., and Lee, J. 2021. Mathematical modeling of heat transfer in y-shaped well couples for developing gas hydrate reservoirs using geothermal energy. *Journal of Natural Gas Science and Engineering* (November 2021). https://doi.org/10.1016/j.jngse.2021.104325

Gates, I., Adams, J. and Larter, S., 2008. The impact of oil viscosity heterogeneity on production from heavy oil and bitumen reservoirs: Geotailoring recovery processes to compositionally graded reservoirs.

Glaso, O., 1980. Generalized pressure-volume-temperature correlations. *Journal of Petroleum Technology*, 32(05), pp.785-795.

Hackley, P.C. and Cardott, B.J. 2016. Application of Organic Petrography in North American Shale Petroleum Systems: A review. *Int J Coal Geol* **163**: 8–51.

John, C.J, Jones, B.L., Moncrief, J.E. et al. 1997. An Unproven Unconventional Seven Billion Barrel Oil Resource—the Tuscaloosa Marine Shale. The Basin Research Institute Bulletin, Baton Rouge, Louisiana, 7: 1–22.

John, C.J., Jones, B.L., Harder, B.J. et al. 2005. Exploratory Progress Towards Proving the Billion Barrel Potential of the Tuscaloosa Marine Shale. GCAGS Trans 55: 367–372.

Li, H., 2020. Effect of viscosity reduction on the production rate of heavy oil: application to soluble gas injection method. *Petroleum Science and Technology*, *38*(3), pp.159-165.

Lohr, C. D., Hackley, P. C., Valentine, B. J., & Enomoto, C. B. 2016. Thermal Gradient Trends in the Tuscaloosa Marine Shale Play Area: Preliminary Results from Studies to Support Oil and Natural Gas Resource Assessments. *Gulf Coast Association of Geological Societies Transactions*, *66*, 1099–1108. Retrieved from http://www.gcags.org/exploreanddiscover/2016/00142_lohr_et_al.pdf

Lohr, C.D. and Hackley, P.C. 2018a. Using Mercury Injection Pressure Analyses to Estimate Sealing Capacity of the Tuscaloosa Marine Shale in Mississippi, USA: Implications for

carbon dioxide sequestration. *Int J Greenh Gas Con* **78**: 375–387. https://doi.org/10.1016/j.ijggc.2018.09.006.

Lu, J., Ruppel, S.C., and Rowe, H.D. 2015. Organic Matter Pores and Oil Generation in the Tuscaloosa Marine Shale. *AAPG Bulletin* **99**(2): 333–357. https://doiorg/10.1306/08201414055.

Luffel, D.L., Hopkins, C.W. and Schettler, P.D., 1993, October. Matrix permeability measurement of gas productive shales. In SPE annual technical conference and exhibition. OnePetro.

Mahdiani, M.R. and Norouzi, M., 2018. A new heuristic model for estimating the oil formation volume factor. Petroleum, 4(3), pp.300-308.

Mancini, E.A. and Puckett, T.M. 2002. Transgressive-Regressive Cycles: Application to Petroleum Exploration for Hydrocarbons Associated with Cretaceous Shelf Carbonates and Coastal and Fluvial-Deltaic Siliciclastics, Northeastern Gulf of Mexico. In Sequence Stratigraphic Models for Exploration and Production: Evolving Methodology, Emerging Models and Application Histories: Presented at the 22nd Annual Bob F. Perkins Research Conference, Houston, Gulf Coast Section, SEPM, 173–199.

Møller, J.B., Meisingset, K.K. and Arief, I.H., 2018, April. An Improved Correlation Approach to Predict Viscosity of Crude Oil Systems on the NCS. In *SPE Norway One Day Seminar*. OnePetro.

Nadooshan, A.A., Eshgarf, H. and Afrand, M., 2018. Measuring the viscosity of Fe3O4-MWCNTs/EG hybrid nanofluid for evaluation of thermal efficiency: Newtonian and non-Newtonian behavior. *Journal of Molecular Liquids*, *253*, pp.169-177.

Nippes, V. 2019. Production Behavior and Decline Curve Analysis of Tuscaloosa Marine Shale Wells in Wilkinson and Amite Counties, Mississippi. Lafayette. University of Louisiana at Lafayette.

Penmatcha, V.R., Arbabi, S. and Aziz, K., 1997, March. Effects of pressure drop in horizontal wells and optimum well length. In *SPE Production Operations Symposium*. OnePetro.

Qun, L.E.I., Yun, X.U., Bo, C.A.I., Baoshan, G.U.A.N., Xin, W.A.N.G., Guoqiang, B.I., Hui, L.I., Shuai, L.I., Bin, D.I.N.G., Haifeng, F.U. and Zheng, T.O.N.G., 2022. Progress and prospects of horizontal well fracturing technology for shale oil and gas reservoirs. *Petroleum Exploration and Development*, *49*(1), pp.191-199.

Ran, Q., Wang, Y., Sun, Y., Yan, L. and Tong, M., 2014. *Volcanic gas reservoir characterization*. Elsevier.

Rutherford, M.S., 1988. Depositional environments and areal distribution of updip Lower Tuscaloosa" Stringer'Member sandstones in portions of Amite and Wilkinson Counties, Mississippi. M. Sc. thesis. In *Unknown Host Publication Title*. University of Southwestern Louisiana, Lafayette, Department of Geology.

Tajali, S. and Arian, M., 2016. Petrophysical Evaluation and the Effect of Shale Layers on Net Pay Zone Thickness in the Marun Oil Field, Iran. Open Journal of Geology, 6(8), pp.763-773.

Thomson, A.R., Kohn, S.C., Prabhu, A. and Walter, M.J., 2021. Evaluating the formation pressure of diamond‐hosted majoritic garnets: A machine learning majorite barometer. Journal of Geophysical Research: Solid Earth, 126(3), p.e2020JB020604.

U.S. Energy Information Administration (EIA). 2021. Review of Emerging Resources: U.S. Shale Gas and Shale Oil Plays. https://www.eia.gov/analysis/studies/usshalegas/ (Accessed 18 August 2022).

U.S. Energy Information Administration (EIA). 2022. Annual Energy Outlook 2022 with Projections to 2050. https://www.eia.gov/outlooks/aeo/ (Accessed 20 April 2022).

Walsh, J.B., 1981, October. Effect of pore pressure and confining pressure on fracture permeability. In International Journal of Rock Mechanics and Mining Sciences & Geomechanics Abstracts (Vol. 18, No. 5, pp. 429-435). Pergamon.

Wood, D.A. and Choubineh, A., 2019. Reliable predictions of oil formation volume factor based on transparent and auditable machine learning approaches. Advances in Geo-Energy Research, 3(3), p.225.

Yang, X. and Guo, B., 2019. A data-driven workflow approach to optimization of fracture spacing in multi-fractured shale oil wells. *Energies*, 12(10), 1973.

Yang, X., Guo, B., 2020. Statistical analyses of reservoir and fracturing parameters for a multi-fractured shale oil reservoir in Mississippi. *Energy Science & Engineering*, 8(3), 616–626.

Yu, W. and Sepehrnoori, K., 2018. *Shale gas and tight oil reservoir simulation*. Gulf Professional Publishing.

Appendix A: Mathematical Modeling of Heat Transfer in Y-shaped Well Couples

Assumptions. Consider the y-shaped well couple shown in Figure 2-2. The following assumptions are made for modeling the heat transfer process:

- The geothermal gradient behind the annulus is not affected by the borehole fluid.
- The heat capacity of fluid is constant.
- Friction-induced heat is negligible.
- The water circulation system can be simplified in four sections, named Section I, Section II, Section III, and Section IV, as depicted in Figure A-1.

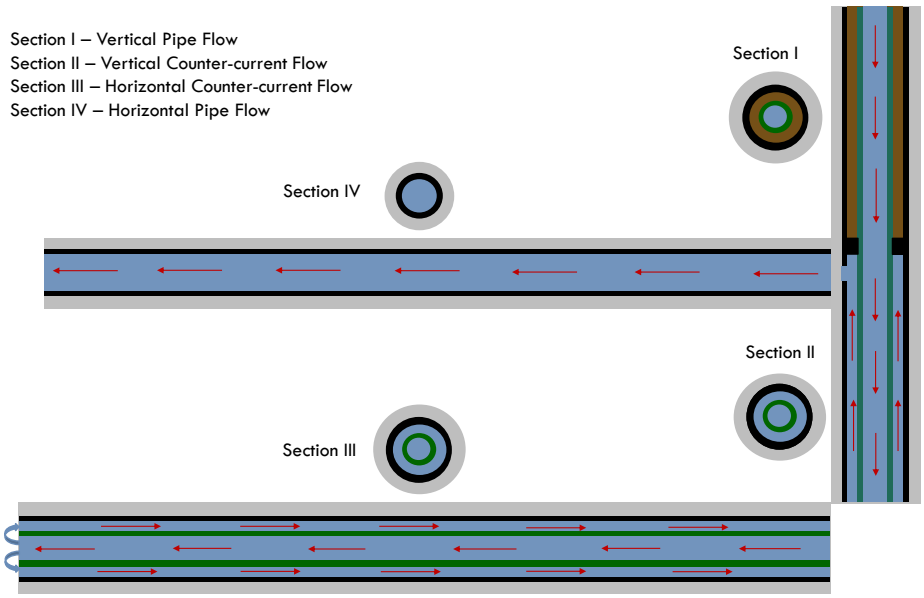

Figure A-1 Wellbore segments in an Y-shaped well couple (Fu et al., 2021)

Governing equation

Section I

Section I includes work pipe, completion fluid in the annulus, casing, and cement sheath between wellbore and casing pipe. Consider the heat flow inside the work pipe of an infinitely small length ΔL during a time period of Δt shown in Figure A-2. The heat balance is given by

$$Q_{p,in} - Q_{p,out} - q_p = Q_{p,chng} \quad \text{(A.1)}$$

where,

$Q_{p,in}$ is the heat source due to convection in J, $Q_{p,out}$ is the flowout heat energy due to convection in J, q_p is lateral heat exchange through the work pipe due to conduction in J, $Q_{p,chng}$ is the external heat exchange through work pipe in J.

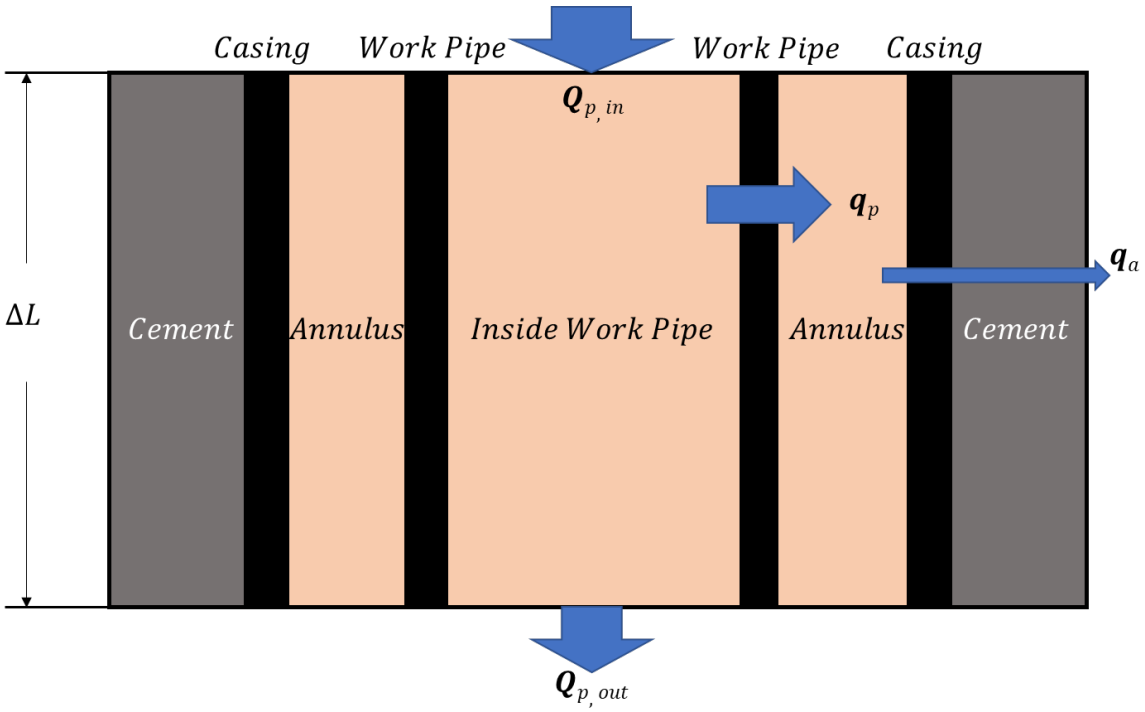

Figure A-2 Heat transfer in Section I

These terms can be further formulated as:

$$Q_{\mathrm{p,in}} = C_{\mathrm{p}}\, \dot{\mathrm{m}}_{\mathrm{p}}\, T_{\mathrm{p,L}}\, \Delta t \tag{A.2}$$

$$Q_{\mathrm{p,in}} = C_{\mathrm{p}}\, \dot{\mathrm{m}}_{\mathrm{p}}\, T_{\mathrm{p,L+\Delta L}}\, \Delta t \tag{A.3}$$

where C_p is the heat capacity of the work fluid inside the pipe in J/kg-^oC, $\dot{m}_p$ is the mass flow rate inside the pipe in kg/s.

Since the work pipe, casing pipe, and cement are much thinner in radial direction than the completion fluid, the heat conduction is dominated by the fluid in the annulus. Therefore,

$$q_p = \pi D_p K_a \Delta L(-\frac{\partial T_p}{\partial r})\Delta t \tag{A.4}$$

where, D_p is the outer diameter of work pipe in m, K_a is the thermal conductivity of annulus fluid in W/m-^oC, and

$$Q_{p,chng} = C_p \rho_p A_p \Delta L \Delta T_p \tag{A.5}$$

where A_p is the inner cross-sectional area of pipe open for fluid flow in m^2, ΔL is an infinitesimal length in m, Δt is an infinitesimal time period in second. Substituting Eqs. (A.2) through (A.5) into Eq. (A.1) gives

$$C_p \dot{m}_p \Delta t (T_{p,L} - T_{p,L+\Delta L}) + \pi D_p K_a \Delta L (\frac{\partial T_p}{\partial r}) \Delta t = \rho_p C_p A_p \Delta L \Delta T_p \tag{A.6}$$

Dividing all the terms of this equation by $\Delta L \Delta t$ yields

$$C_p \dot{m}_p \frac{(T_{p,L} - T_{p,L+\Delta L})}{\Delta L} + \pi D_p K_a \frac{\partial T_p}{\partial r} = \rho_p C_p A_p \frac{\Delta T_p}{\Delta t} \tag{A.7}$$

For an infinitesimal ΔL and Δt, this equation becomes

$$\frac{\partial T_p}{\partial L} + \frac{\rho_p A_p}{\dot{m}_p} \frac{\partial T_p}{\partial t} = \frac{\pi D_p K_a}{C_p \dot{m}_p} \frac{\partial T_p}{\partial r} \tag{A.8}$$

The radial-temperature gradient in the annulus can be formulated as

$$\frac{\partial T_p}{\partial r} = \frac{T_g - T_p}{t_a} \tag{A.9}$$

where T_g is the geothermal temperature at target depth in ◦C, t_a is the thickness of annulus in m.

Assuming that the linear geo-temperature is expressed by

$$T_g = T_{g0} + GL \tag{A.10}$$

Substituting Eqs. (A.9) and (A.10) into Eq. (A.8) yields

$$\frac{\partial T_p}{\partial L} + \lambda_p \frac{\partial T_p}{\partial t} + \alpha_{p1} (T_p - T_{g0} - GL) = 0 \tag{A.11}$$

where,

$$\lambda_p = \frac{\rho_p A_p}{\dot{m}_p} \tag{A.12}$$

$$\alpha_{p1} = \frac{\pi D_p K_a}{C_p \dot{m}_p t_a} \tag{A.13}$$

Since the flow is the steady flow, Eq. (A.11) degenerates to

$$\frac{dT_p}{dL} + \alpha_{p1} T_p + \beta L + \gamma = 0 \quad \text{(A.14)}$$

where,

$$\beta = -\alpha_{p1} G \quad \text{(A.15)}$$

$$\gamma = -\alpha_{p1} T_{g0} \quad \text{(A.16)}$$

Subjected to the boundary condition of

$$T_p = T_{p0} \, at \, L = 0 \quad \text{(A.17)}$$

Eq. (A.14) has a solution of the following form (Li et al., 2015):

$$T_p = \frac{1}{\alpha_{p1}^2} [\beta - \alpha_{p1} \beta L - a_{p1} \gamma + e^{-\alpha_{p1}(L+C)}] \quad \text{(A.18)}$$

where,

$$C = -\frac{1}{\alpha_{p1}} \ln [-\beta + \alpha_{p1}^2 T_{p0} + \alpha_{p1} \gamma] \quad \text{(A.19)}$$

The fluid temperature at the end of section ($L = L_1$) is expressed as

$$C = -\frac{1}{\alpha_{p1}} \ln [-\beta + \alpha_{p1}^2 T_{p0} + \alpha_{p1} \gamma] \quad \text{(A.20)}$$

Section III

Temperature in the Section III affects the temperature in the Section II, so the mathematic model of the temperature in the Section III is developed first. The Section II consists of work pipe, work fluid, casing, and cement sheath as shown in Figure A-3. Consider the heat flow inside the work pipe of length ΔL during a time of Δt. Eqs (A.1), (A.2), (A.3), and (A.5) are the same as Section I. However, Eq. (A.4) is given as follows:

$$q_p = \pi d_p K_p \Delta L (-\frac{\partial T_p}{\partial r}) \Delta t \quad \text{(A.21)}$$

where d_p is the inner diameter of work pipe in m, K_p is the thermal conductivity of pipe in W/m-^oC.

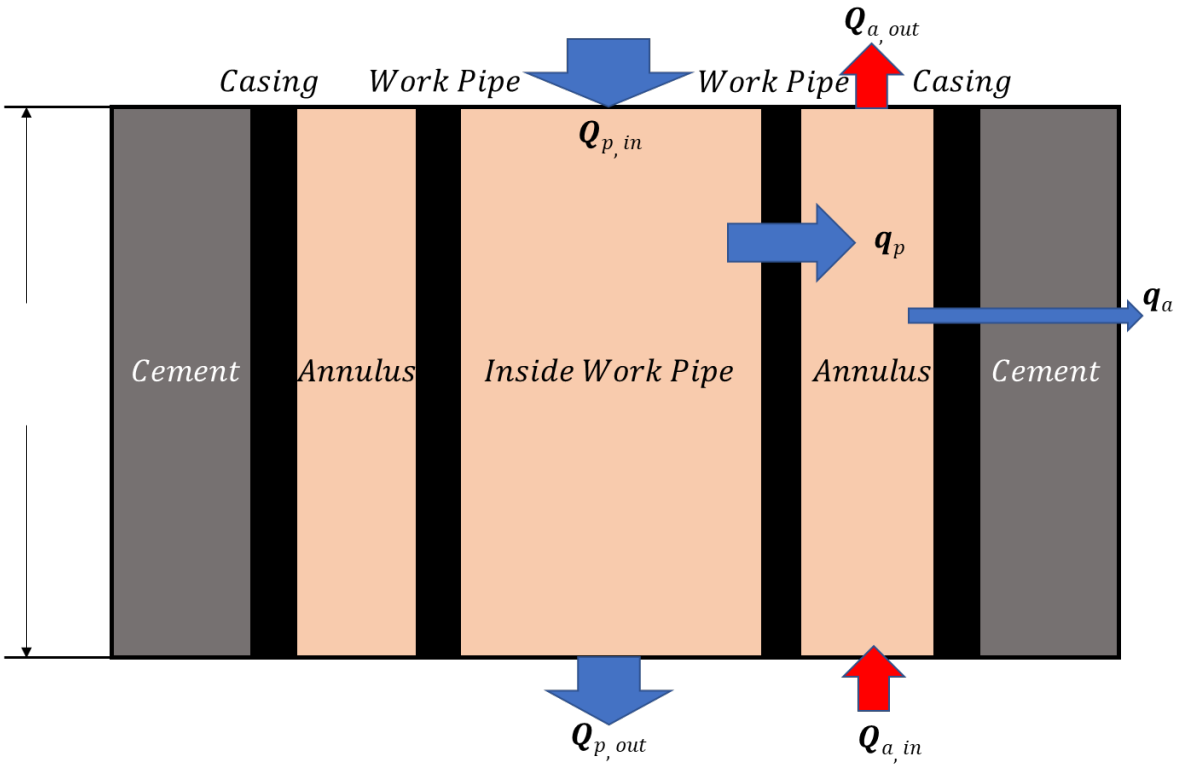

Figure A-3 Heat transfer in Section II and Section III

Substituting Eqs. (A.2), (A.3), (A.21), and (A.5) into Eq. (A.1) gives

$$C_p \dot{m}_p \Delta t(T_{p,L} - T_{p,L+\Delta L}) + \pi D d_p K_p \Delta L(\frac{\partial T_p}{\partial r})\Delta t = \rho_p C_p A_p \Delta L \Delta T_p \tag{A.22}$$

Dividing all the terms of this equation by $\Delta L \Delta t$ yields

$$C_p \dot{m}_p \frac{(T_{p,L} - T_{p,L+\Delta L})}{\Delta L} + \pi d_p K_p \frac{\partial T_p}{\partial r} = \rho_p C_p A_p \frac{\Delta T_p}{\Delta t} \tag{A.23}$$

For an infinitesimal of ΔL and Δt, this equation becomes

$$\frac{\partial T_p}{\partial L} + \frac{\rho_p A_p}{\dot{m}_p}\frac{\partial T_p}{\partial t} = \frac{\pi d_p K_p}{C_p \dot{m}_p}\frac{\partial T_p}{\partial r} \tag{A.24}$$

The radial-temperature gradient in the pipe can be formulated as

$$\frac{\partial T_p}{\partial r} = \frac{T_a - T_p}{t_p} \tag{A.25}$$

Where T_a is fluid temperature in the annulus at target depth in ◦C, t_p is the thickness of work pipe in m.

Substituting Eq. (A.25) into Eq. (A.24) and rearranging the latter yield

$$\frac{\partial T_p}{\partial L} + \lambda_p \frac{\partial T_p}{\partial t} + \alpha_{p3}(T_p - T_a) = 0 \quad \text{(A.26)}$$

where,

$$\lambda_p = \frac{\rho_p A_p}{\dot{m}_p} \quad \text{(A.27)}$$

$$\alpha_{p3} = \frac{\pi d_p K_p}{C_p \dot{m}_p t_p}. \quad \text{(A.28)}$$

For the heat flow in the annulus during a time of Δt, the heat balance is given by

$$Q_{\mathrm{p,in}} - Q_{\mathrm{a,out}} + q_{\mathrm{p}} - q_{\mathrm{a}} = Q_{\mathrm{a,chng}} \quad \text{(A.29)}$$

where $Q_{p,in}$ is the heat source due to convection in J, $Q_{p,out}$ is the flow out heat energy due to convection in J, q_p is lateral heat exchange through the work pipe due to conduction in J, $Q_{p,chng}$ is the external heat exchange through work pipe in J, q_a is lateral heat exchange through the casing pipe due to conduction in J.

These terms can be further formulated as

$$Q_{a,in} = C_a \dot{m}_a T_{a,L+\Delta L} \Delta t \quad \text{(A.30)}$$

$$Q_{a,out} = C_a \dot{m}_a T_{a,L} \Delta t \quad \text{(A.31)}$$

$$q_p = \pi d_p K_p \Delta L(-\frac{\partial T_p}{\partial r})\Delta t \quad \text{(A.32)}$$

$$q_a = \pi d_c K_c \Delta L(-\frac{\partial T_a}{\partial r})\Delta t \quad \text{(A.33)}$$

$$Q_{a,chng} = C_a \rho_a A_a \Delta L \Delta T_a \quad \text{(A.34)}$$

Substituting Eqs. (A.30) through (A.34) into Eq. (A.29) gives

$$C_a \dot{m}_a \Delta t(T_{a,L+\Delta L} - T_{a,L}) - \pi d_p K_p \Delta L(\frac{\partial T_p}{\partial r})\Delta t + \pi d_c K_c \Delta L(\frac{\partial T_a}{\partial r})\Delta t = \rho_a C_a A_a \Delta L \Delta T_a \quad \text{(A.35)}$$

Dividing all the terms of this equation by $\Delta L \Delta t$ yields

$$C_a \dot{m}_a \frac{(T_{a,L+\Delta L} - T_{a,L})}{\Delta L} - \pi d_p K_p (\frac{\partial T_p}{\partial r}) + \pi d_c K_c (\frac{\partial T_a}{\partial r}) = \rho_a C_a A_a \frac{\Delta T_a}{\Delta t} \quad \text{(A.36)}$$

For an infinitesimal of ΔL and Δt, this equation becomes

$$C_a \dot{m}_a \frac{(T_{a,L+\Delta L} - T_{a,L})}{\Delta L} - \pi d_p K_p (\frac{\partial T_p}{\partial r}) + \pi d_c K_c (\frac{\partial T_a}{\partial r}) = \rho_a C_a A_a \frac{\Delta T_a}{\Delta t} \quad \text{(A.37)}$$

The radial-temperature gradients in the pipe and cement can be formulated as

$$\frac{\partial T_p}{\partial r} = \frac{T_a - T_p}{t_p} \quad \text{(A.38)}$$

$$\frac{\partial T_a}{\partial r} = \frac{T_{g3} - T_a}{t_c} \quad \text{(A.39)}$$

where T_{g4} is the average geo-temperature in the Section III. Substituting Eqs. (A.38) and (A.39) into Eq. (A.37) yields

$$\frac{\partial T_a}{\partial L} - \lambda_{a3} \frac{\partial T_a}{\partial t} + \beta_{a3}(T_p - T_a) - \alpha_{a3}(T_a - T_{g3}) = 0 \quad \text{(A.40)}$$

where,

$$\lambda_{a3} = \frac{\rho_a A_a}{\dot{m}_a} \quad \text{(A.41)}$$

$$\beta_{a3} = \frac{\pi d_p K_p}{C_a \dot{m}_a t_p} \quad \text{(A.42)}$$

$$\alpha_{a3} = \frac{\pi d_c K_c}{C_a \dot{m}_a t_c} \quad \text{(A.43)}$$

The time-dependent temperatures T_p and T_a at any given depth can be solved numerically from Eqs. (A.26) and (A.40). For steady heat flow, Eqs.

(A.26) and (A.40) can be written as:

$$\frac{\partial T_p}{\partial L} + \alpha_{p3}(T_p - T_a) = 0 \quad \text{(A.44)}$$

$$\frac{\partial T_a}{\partial L} + \beta_{a3}(T_p - T_a) - \alpha_{a3}(T_a - T_{g3}) = 0 \quad \text{(A.45)}$$

The boundary conditions for solving Eqs. (A.44) and (A.45) are expressed as

$$T_p = T_{p2} \; at \; L = L_2 \quad \text{(A.46)}$$

$$T_a = T_p \; at \; L = L_3 \tag{A.47}$$

The governing equations (A.44) and (A.45) subjected to the boundary conditions (A.46) and (A.47) were solved with the method of characteristics. The solutions take the following form (Guo et al., 2017):

$$T_p = C_1 A e^{r_1 L} + C_2 A e^{r_2 L} + b \tag{A.48}$$

$$T_a = C_1 (A + r_1) e^{r_1 L} + C_2 (A + r_2) e^{r_2 L} + b \tag{A.49}$$

where,

$$C_1 = \frac{AB(C-b) r_2 e^{r_2 L_3}}{A^2 B (r_1 e^{r_1 L_3} - r_2 e^{r_2 L_3})} \tag{A.50}$$

$$C_2 = \frac{AB(C-b) r_1 e^{r_1 L_3}}{A^2 B (r_1 e^{r_1 L_3} - r_2 e^{r_2 L_3})} \tag{A.51}$$

where,

$$r_1 = \frac{B+E-A+\sqrt{(B+E-A)^2+4AB}}{2} \tag{A.52}$$

$$r_2 = \frac{B+E-A-\sqrt{(B+E-A)^2+4AB}}{2} \tag{A.53}$$

where $A = \alpha_{p3}$, $B = \alpha_{a3}$, $C = T_{p2}$, $E = \beta_{a3}$, $b = T_{g3}$.

The temperatures at the beginning of section ($L = 0$) are

$$T_{p2} = A(C_1 + C_2) + b \tag{A.54}$$

$$T_{a2} = C_1 (A + r_1) + C_2 (A + r_2) + b \tag{A.55}$$

The temperature difference between the inside and outside of the pipe at the top of the section is:

$$\Delta T = T_{a2} - T_{p2} = C_1 r_1 + C_2 r_2 \tag{A.56}$$

Section II

Figure A-3 shows the Section II which consists of work pipe, work fluid, casing, and cement sheath. The model derivation for the Section III is the same as the Section II up to Eq. (A.38).

The radial-temperature gradient in the cement sheath can be formulated as

$$\frac{\partial T_a}{\partial r} = \frac{T_g - T_a}{t_c} \tag{A.57}$$

Therefore Eq. (A.37) becomes

$$\frac{\partial T_a}{\partial L} - \lambda_{a2}\frac{\partial T_a}{\partial t} + \beta_{a2}(T_p - T_a) - \alpha_{a2}(T_a - T_g) = 0 \tag{A.58}$$

where,

$$\lambda_{a2} = \frac{\rho_a A_a}{\dot{m}_a} \tag{A.59}$$

$$\beta_{a2} = \frac{\pi d_p K_p}{C_a \dot{m}_a t_p} \tag{A.60}$$

$$\alpha_{a2} = \frac{\pi d_c K_c}{C_a \dot{m}_a t_c} \tag{A.61}$$

The temperatures T_p and T_a at any given depth can be solved numerically from Eqs. (A.26) and (A.58). For steady heat flow, Eqs. (A.26) and (A.58) can be written as:

$$\frac{\partial T_p}{\partial L} + \alpha_{p2}(T_p - T_a) = 0 \tag{A.62}$$

$$\frac{\partial T_a}{\partial L} + \beta_{a2}(T_p - T_a) - \alpha_{a2}(T_a - T_g) = 0 \tag{A.63}$$

where the geo-temperature can be expressed as:

$$T_g = T_{g0} + G(L_1 + L) \tag{A.64}$$

The boundary conditions for solving Eqs. (A.62) and (A.63) are expressed as

$$T_p = T_{p1}\ at\ L = L_0 \tag{A.65}$$

$$T_a = T_p + \Delta T\ at\ L = L_2 \tag{A.66}$$

The governing equations (A.62) and (A.63) subjected to the boundary conditions of (A.65) and (A.66) are solved with the method of characteristics. The solutions take the following form:

$$T_p = C_1' A' e^{r_1 L} + C_2' A' e^{r_2 L} + a'L + \frac{A'a' + A'B'b' - a'(B' + E')}{A'B'} \tag{A.67}$$

$$T_a = C_1'(A' + R_1)e^{R_1 L} + C_2'(A' + R_2)e^{R_2 L} + a'L + \frac{A'a' + A'B'b' - a'E'}{A'B'} \tag{A.68}$$

where,

$$C_1' = \frac{A'B'(A'D'-a')-[A'B'C'-A'B'b'-A'a'+a'(B'+E')]R_2 e^{R_2 L_2}}{A'2B'(R_1 e^{R_1 L_2}-R_2 e^{R_2 L_2})} \quad \text{(A.69)}$$

$$C_2' = \frac{-A'B'(A'D'-a')-[A'B'C'-A'B'b'-A'a'+a'(B'+E')]R_1 e^{R_1 L_2}}{A'2B'(R_1 e^{R_1 L_2}-R_2 e^{R_2 L_2})} \quad \text{(A.70)}$$

$$R_1 = \frac{B'+E'-A'+\sqrt{(B'+E'-A')^2+4A'B'}}{2} \quad \text{(A.71)}$$

$$R_2 = \frac{B'+E'-A'-\sqrt{(B'+E'-A')^2+4A'B'}}{2} \quad \text{(A.72)}$$

where $A' = \alpha = \alpha$, $B' = \alpha$, $C' = T$, $D' = \Delta T$, $E' = \beta$, $a' = G$, and $b' = T$.

Section IV

The Section IV includes well casing pipe, work fluid, and cement sheath as shown in Figure A-4.

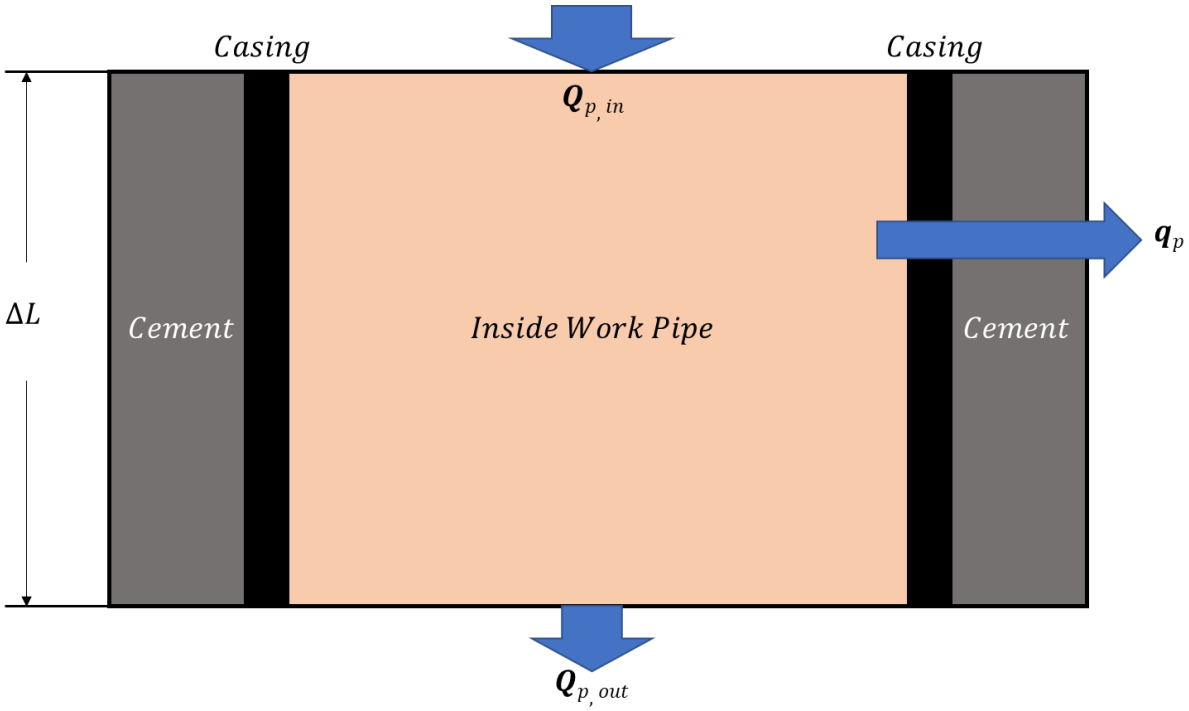

Figure A-4 Heat transfer in Section IV

Consider the heat flow inside the cased hole of length ΔL during a time of Δt. The heat balance is given by

$$Q_{p,in} - Q_{p,out} + q_p = Q_{p,chng} \tag{A.73}$$

where $Q_{p,in}$ is the heat source due to convection in J, $Q_{p,out}$ is the flow out heat energy due to convection in J, q_p is lateral heat exchange through the work pipe due to conduction in J, $Q_{p,chng}$ is the external heat exchange through work pipe in J.

These terms can be further formulated as:

$$Q_{p,in} = C_p \dot{m}_p T_{p,L} \Delta t \tag{A.74}$$

$$Q_{p,out} = C_p \dot{m}_p T_{p,L+\Delta L} \Delta t \tag{A.75}$$

where Cp is the heat capacity of the work fluid inside the pipe in J/kg-^oC, $\dot{m}_p$ is the mass flow rate inside the pipe in kg/s.

Since the casing pipe is much thinner than the cement sheath, the heat conduction is dominated by the cement sheath. Therefore,

$$q_p = \pi D_{csg} K_c \Delta L (-\frac{\partial T_p}{\partial r}) \Delta t \tag{A.76}$$

where, D_{csg} is the outer diameter of the casing (inner diameter of cement sheath) in m, Kc is the thermal conductivity of cement sheath in W/m-^oC. And

$$Q_{p,chng} = C_p \rho_p A_{csg} \Delta L \Delta T_p \tag{A.77}$$

where, A_{csg} is the inner cross-sectional area of casing open for fluid flow in m^2. Substituting Eqs. (A.74) through (A.77) into Eq. (A.73) gives

$$C_p \dot{m}_p \Delta t (T_{p,L} - T_{p,L+\Delta L}) + \pi D_{csg} K_c \Delta L (\frac{\partial T_p}{\partial r}) \Delta t = \rho_p C_p A_{csg} \Delta L \Delta T_p \tag{A.78}$$

Dividing all the terms of this equation by $\Delta L \Delta t$ yields

$$C_p \dot{m}_p \frac{(T_{p,L} - T_{p,L+\Delta L})}{\Delta L} + \pi D_{csg} K_c \frac{\partial T_p}{\partial r} = \rho_p C_p A_{csg} \frac{\Delta T_p}{\Delta t} \tag{A.79}$$

For an infinitesimal of ΔL and Δt, this equation becomes

$$\frac{\partial T_p}{\partial L} + \frac{\rho_p A_{csg}}{\dot{m}_p} \frac{\partial T_p}{\partial t} = \frac{\pi D_{csg} K_c}{C_p \dot{m}_p} \frac{\partial T_p}{\partial r} \tag{A.80}$$

The radial-temperature gradient in the cement sheath can be formulated as

$$\frac{\partial T_p}{\partial r} = \frac{T_{g4} - T_p}{t_c} \tag{A.81}$$

where T_{g4} is the average geothermal temperature at the depth of the section in ◦C， T_c is the thickness of cement sheath in m. Substituting Eq. (A.81) into Eq. (A.80) yields

$$\frac{\partial T_p}{\partial L} + \lambda_{p4} \frac{\partial T_p}{\partial t} + \alpha_{csg}(T_p - T_{g4}) = 0 \tag{A.82}$$

where,

$$\lambda_{p4} = \frac{\rho_p A_{csg}}{\dot{m}_p} \tag{A.83}$$

$$\alpha_{csg} = \frac{\pi D_{csg} K_c}{C_p \dot{m}_p t_c} \tag{A.84}$$

Under steady flow conditions, Eq. (A.82) degenerates to

(A.84)

$$\frac{dT_p}{dL} + \alpha_{csg} T_p + \gamma_{csg} = 0 \tag{A.85}$$

where,

$$\gamma_{csg} = -\alpha_{csg} T_{g4} \tag{A.86}$$

Subjected to the boundary condition of

$$T_p = T_{a1} \; at \; L = 0 \tag{A.87}$$

where T_{a1} is the annular temperature at the top of section II. Eq. (A.85) has a solution of the following form:

$$T_p = \frac{1}{\alpha_{csg}} [(\alpha_{csg} T_{a1} + \gamma_{csg}) e^{-\alpha_{cgg} L} - \gamma_{csg}] \tag{A.88}$$

Appendix B: Mathematical Modeling of Heat Transfer in TMS Reservoirs

Assumptions. Consider the horizontal heat dissipator wellbore shown in Figure 2-1. The following assumptions are made for modeling the heat transfer process:

- The reservoir is homogeneous and isotropic with constant density, thermal conductivity, and specific heat.
- The reservoir is considered infinitely large as compared to the wellbore size.

Governing Equation. The governing equation of temperature is the commonly known diffusivity equation expressed as

$$\frac{1}{r}\frac{\partial}{\partial r}\left(r\frac{\partial T}{\partial r}\right)=\frac{1}{\beta}\frac{\partial T}{\partial t} \tag{B.1}$$

where T is temperature in ^{o}C, r is distance from the wellbore center line in meter, t is time in second, and b is thermal diffusivity constant defined by

$$\beta=\frac{K}{\rho_s C_{ps}} \tag{B.2}$$

where K is thermal conductivity in W/m-^{o}C, r is density in kg/m^3, C_{ps} is specific heat in J/kg-^{o}C.

Boundary Conditions. The initial condition is expressed as

$$T=T_i \quad \text{at } t=0 \text{ for all } r. \tag{B.3}$$

where T_i is initial reservoir temperature. The boundary condition at the wellbore is expressed as

$$q_{r_w}=-K\left[\frac{dT}{dr}\right]_{r=r_w} \quad \text{for all } t. \tag{B.4}$$

where q_{rw} is rate of flow of heat per unit time per unit area of wellbore in J/s-m^2. For a circular wellbore with radius r_w and length L, the following relation holds true:

$$q_{r_w} = \frac{Q_{r_w}}{2\pi r_w L} \tag{B.5}$$

where Q_{rw} is rate of flow of heat per unit time in J/s. Substituting Eq. (A.5) into Eq. (A.4) and rearranging the latter gives

$$\frac{Q_{r_w}}{2\pi LK} = -r_w \left[\frac{dT}{dr}\right]_{r=r_w} \quad \text{for all } t. \tag{B.6}$$

Solution

The solution of Eq. (A.1) is sought by Boltzmann's transformation:

$$s = \frac{r^2}{4\beta t} \tag{B.7}$$

So that

$$\frac{\partial s}{\partial r} = \frac{r}{2\beta t} \tag{B.8}$$

and

$$\frac{\partial s}{\partial t} = -\frac{r^2}{4\beta t^2} \tag{B.9}$$

Substituting Eqs. (B.7) through (B.9) into Eq. (B.1) and rearranging the latter give

$$\frac{dT}{ds} + s\frac{d}{ds}\left(\frac{dT}{ds}\right) = -s\frac{dT}{ds}. \tag{B.10}$$

Let

$$\frac{dT}{ds} = T' \tag{B.11}$$

then Eq. (B.10) becomes

$$T' + s\frac{dT'}{ds} = -sT' \tag{B.12}$$

or

$$\frac{dT'}{T'} = -\frac{s+1}{s}ds \tag{B.13}$$

which is integrated to obtain

$$lnT' = -lns - s + c_1 \tag{B.14}$$

where c_1 is an integration constant. This equation is rearranged to give

$$T' = c_2\frac{e^{-s}}{s} \tag{B.15}$$

where c_2 is a constant.

Chain rule gives

$$r\frac{dT}{dr} = r\frac{dT}{ds}\frac{ds}{dr} \tag{B.16}$$

Chain rule gives

$$r\frac{dT}{dr} = r\frac{dT}{ds}\frac{ds}{dr} = r\frac{dT}{ds}\left(\frac{r}{2\beta t}\right) = \frac{dT}{ds}\left(\frac{r^2}{2\beta t}\right) = 2s\frac{dT}{ds} \tag{B.17}$$

Substituting Eq. (B.15) into Eq. (B.17) gives

$$r\frac{dT}{dr} = 2c_2e^{-s} \tag{B.18}$$

At wellbore where s approaches 0, this relation becomes

$$r_w\left[\frac{dT}{dr}\right]_{r=r_w} = 2c_2 \tag{B.19}$$

Applying boundary condition Eq. (B.6) to Eq. (B.19) yields

$$\frac{Q_{r_w}}{2\pi LK} = -2c_2 \tag{B.20}$$

which gives

$$c_2 = -\frac{Q_{r_w}}{4\pi LK} \tag{B.21}$$

Substituting Eq. (B.21) into eq. (B.15) gives

$$\frac{dT}{ds} = -\frac{Q_{r_w}}{4\pi LK}\frac{e^{-s}}{s} \tag{B.22}$$

which is integrated over time:

$$\int_{T_i}^{T} dT = -\frac{Q_{r_w}}{4\pi LK}\int_{\infty}^{s}\frac{e^{-s}}{s}ds \tag{B.23}$$

or

$$T = T_i - \frac{Q_{r_w}}{4\pi LK}\int_{\infty}^{s}\frac{e^{-s}}{s}ds = T_i + \frac{Q_{r_w}}{4\pi LK}\int_{s}^{\infty}\frac{e^{-s}}{s}ds \tag{B.24}$$

i.e.,

$$T = T_i + \frac{Q_{r_w}}{4\pi LK}E_i(s) \tag{B.25}$$

The heat flow rate from wellbore to reservoir can be calculated by

$$Q_{rw} = C_{pl}\dot{m}_p(T_{in} - T_{out}) \tag{B.26}$$

where C_{pl} is the heat capacity of the fluid inside the wellbore in $J/(kg \cdot ℃)$, $\dot{m}_p$ is the mass flow rate inside the wellbore in kg/s, and T_{in} and T_{out} are fluid temperatures in ℃ at the inlet and outlet of the wellbore, respectively.

Appendix C: Matlab Program- Temperature Profile in TMS reservoir

```
clc;

clear;

% heat capacity of fluid, J/(kg*degC)

Cp=4200;

% mass flow rate, kg/s

mp=0.515;

% distance from wellbore to formation, m

L=10;

% thermal conductivity of the rock, W/(m*degC)

K= 2.5;

% initially formation temperature, degC

Ti=99.2;

% heat capacity of the rock, J/(kg*degC)

c=1500;

% density of the rock, kg/m^3

Rho=2800;

% flow in temperature, degC

Tin=104.7;

% flow out temperature, degC

Tout=99.2;

Qrw=Cp*mp*(Tin-Tout)

m=Qrw/(4*pi*L*K)

r=0.3:0.5:10

Beta = K/(Rho*c);
```

```
% working time, a changable value, day

day=1;

% transfer days to seconds,  1 day = 86400 s

t = 86400*day;

s=r.^2/(4*Beta*t)

Y = expint(s)

%T is the temperature we need, degC.

T =Ti + Qrw/(4*pi*L*K)*Y

plot(r,T)

xlabel('Distance (m)')

ylabel('Reservoir temperature (degC)')

title("Temperature profile in TMS reservoir"
```

Biographical Sketch

He Zhang was born in Beijing, China. He received the bachelor's degree in petroleum engineering from the China University of Petroleum, in 2008, the master's degree in mathematics from Texas A&M University-Commerce, USA, in 2016, and the master's degree in petroleum engineering from the University of Louisiana at Lafayette, USA, in 2019. Then he entered the PhD program in Systems Engineering at the University of Louisiana, Lafayette. He graduated in the Summer 2022 with a Doctor of Philosophy degree in systems engineering with a concentration in petroleum engineering. He was also a Drilling Supervisor with six years of experience in engineering at China National Offshore Oil Corporation.